Water Resources Research

RESEARCH ARTICLE
10.1029/2023WR035937

The Evolution of Hillslope Hydrology: Links Between Form, Function and the Underlying Control of Geology

Anne Hartmann[1] and **Theresa Blume**[1]

[1]GFZ German Research Centre for Geosciences, Section Hydrology, Potsdam, Germany

Key Points:

- The underlying geology controls landscape evolution in glacial forefields
- After 10,000 years of evolution, hillslope form and hydrological functioning differ between the calcareous and siliceous sites
- Soil pH is a key variable indicative of differences in soil evolution and hydrological response between the two forefields

Correspondence to:

A. Hartmann,
aha@gfz-potsdam.de

Citation:

Hartmann, A., & Blume, T. (2024). The evolution of hillslope hydrology: Links between form, function and the underlying control of geology. *Water Resources Research*, *60*, e2023WR035937. https://doi.org/10.1029/2023WR035937

Received 26 JUL 2023
Accepted 12 DEC 2023

Author Contributions:

Conceptualization: Anne Hartmann, Theresa Blume
Data curation: Anne Hartmann
Formal analysis: Anne Hartmann
Funding acquisition: Theresa Blume
Investigation: Anne Hartmann
Methodology: Anne Hartmann
Project Administration: Theresa Blume
Supervision: Theresa Blume
Validation: Anne Hartmann, Theresa Blume
Visualization: Anne Hartmann
Writing – original draft: Anne Hartmann
Writing – review & editing: Anne Hartmann, Theresa Blume

Abstract Form and function are two major characteristics of hydrological systems. While form summarizes the structure of the system, function represents the hydrological response. Little is known about how these characteristics evolve and how form relates to function in young hydrological systems. We investigated how form and function evolve during the first millennia of landscape evolution. We analyzed two hillslope chronosequences in glacial forelands, one developed from siliceous and the other from calcareous parent material. Variables describing hillslope form included soil physical properties, surface, and vegetation characteristics. Variables describing hydrological function included soil water response times, soil water storage, drainage, and dominant subsurface flow types. We identified links between form and hydrological function via cluster analysis. Clusters identified based on form were compared in terms of their hydrological functioning. The comparison of the two different parent materials shows how strongly landscape evolution is controlled by the underlying geology. Soil pH appears to be a key variable influencing vegetation, soil formation and subsequently hydrology. At the calcareous site, the high buffering capacity of the soil leads to less soil formation and fast, vertical subsurface water transport dominates the water redistribution even after more than 10,000 years of landscape evolution. At the siliceous site, soil acidification results in accumulation of organic material, a high water storage capacity, and in podsolization. Under these conditions water redistribution changes from vertical subsurface water transport at the young age classes to water storage in the organic surface layer and lateral subsurface water transport within 10,000 years.

1. Introduction

As hillslopes are the largest functional components of catchments, their characteristics and functioning have a major impact on the overall hydrological catchment response. Over 95% of stream water is transported through hillsides in the form of subsurface or overland flow (Kirkby, 1988). Based on its function to store and to release water, soil plays a key role in the hillslope hydrological response and provides important ecosystem services (Clothier et al., 2008). For example, soil can store large amounts of water, which reduces flood risk and is valuable for agricultural purposes. The soil's ability to feed streams during dry seasons by slowly releasing water (Nippgen et al., 2016) is vital to both ecosystems and humans.

The hydrologic response of hillslopes depends on soil water dynamics and subsurface flow paths during rainfall events, influenced by soil and surface characteristics of the hillslopes (Blume et al., 2009; Lohse & Dietrich, 2005; Wlostowski et al., 2021). Since hillslope structure varies spatially (Nahar et al., 2004), the spatial variability of the hydrological response is also high. Hydrologic processes furthermore develop and change over the years due to landscape evolution (i.e., weathering, soil development, vegetation succession) and the associated changes in the hillslope/soil structure. The spatial variability of the hydrological responses has been a focal point in numerous studies (e.g., Brocca et al., 2007; Maeda et al., 2006; Singh et al., 2021). Investigations into the temporal variability encompass aspects such as seasonal variations (Kim, 2009; Wilson et al., 2004), the temporal variability of driving forces and corresponding responses, and the impacts of land use changes (Sajikumar & Remya, 2015; Truong et al., 2022; Wojkowski et al., 2022). However, moving from multi-year or even decadal studies to the time scale of landscape evolution provides a very different challenge.

The understanding of how the hydrological response co-evolves with hillslope structure is crucial for the evaluation of how hydrological systems will adapt to changes in climate (Montagne & Cornu, 2010) or anthropogenic disturbances (Cui et al., 2021). Human activities, such as changes in land cover and use, landscape degradation, and anthropogenic climate change, have a profound impact on water quantity, quality, and temporal availability (Bronstert et al., 2002; Jin et al., 2021). Glacier retreat, bark beetle infestations, surface mine closures, land

conversion for agriculture, and diverse land use practices are only a few examples which can profoundly influence local hydrology (Goeking & Tarboton, 2020; Haeberli, 2017; Ross et al., 2021; Truong et al., 2022). These extreme interventions in hydrological systems will shape future landscapes significantly different from their past and present states, challenging the notion of hydrological systems as stationary (Ehret et al., 2014). For example, the exposure of previously glaciated areas initiates vegetation growth and soil formation, co-evolving with hillslope morphology and soil water movement. This process leads to hydrological system alterations within centuries to millennia (D'Amico et al., 2014; Egli et al., 2006, 2008).

To accurately predict the evolution of water flow in hydrological systems, it is essential to identify feedback processes that influence the co-evolution of biota, soil, and water transport. Landscape evolution models serve as valuable tools to explore how landscapes will evolve in response to changes in driving forces. Litwin et al. (2022) for example, introduced a landscape evolution model that links landscape form and hydrological function by integrating feedback between runoff generation and surface erosion. However, the model does not include ecological processes, which evolve in conjunction with hydrological processes and the resulting feedback cycles between them. Due to the absence of field observations, soil landscape evolution models are still forced to ignore crucial subsurface water transport processes, such as preferential flow and lateral flow, and how these processes co-evolve with soil and vegetation characteristics (van der Meij et al., 2018), which can lead to incorrectly modeled transport and relocation processes during landscape evolution (Sauer et al., 2012).

A few studies examined the hydrological response of soils of different ages in volcanic landscapes and linked the changes to substantial alterations in soil structure. Lohse and Dietrich (2005) for example, found differences in the catchment response of a 300-year-old Andisol and a 4.1 million year-old Oxisol. While the younger soil was coarse textured and drained freely via mainly vertical water transport, the old soil showed a decrease in permeability and mainly lateral flow due to the accumulation of secondary clay minerals. Comparing Holocene and Late Pleistocene lava landscapes, Jefferson et al. (2010) observed a reduction in base flow and an increase in lateral shallow underground flow and surface runoff. The same trend of lower base flow, more shallow subsurface flow, and more flashy runoff with catchment age was noted by Yoshida and Troch (2016), who compared 14 volcanic catchments ranging in age from 0.225 to 82.2 million years. They also relate the changes to the formation of impermeable layers as a result of progressive chemical weathering.

Comparable studies in other geologies are hard to find. Geology as a catchment (or landscape) forming factor (Troch et al., 2015) has a big impact on the co-evolution of landscapes. Observations made in a specific geology should not be simply transferred to other geologies. The physical and chemical properties of the parent material directly or indirectly influence the hydrological response. For example, the bedrock permeability directly impacts the hydrologic storage and release of catchments, as it was shown that a higher bedrock permeability leads to higher storage and base flow, but dampened peak flow (Pfister et al., 2017). The weatherability and chemical composition of the geology (parent material) indirectly affect the hydrologic response as they are primary controls for soil development (Jenny, 1941) and define the physical properties (e.g., texture, bulk density, porosity, water holding capacity) and consequently the hydrologic properties and processes (Heidbüchel et al., 2013; Lin, 2003) of the regolith and soil. However, in the evolution process, the soils also interact with other factors such as vegetation and water. The interplay between soil and water regulates the vegetation density and composition by providing nutrients in concentrations that can either limit or enhance plant growth (Hahm et al., 2014). Vegetation in turn also affects soil development and thus the hydrological response (Bonetti et al., 2021). For example, the development of organic layers can immensely increase water storage (Ramírez et al., 2017) and facilitate lateral subsurface flow (Y. Yang et al., 2012).

Especially in mountain regions, where the accelerated retreat of glaciers exposes more and more young landscapes, structural changes during a time span of a few centuries to a thousand years can be striking. Initial signs of soil development can be observed in as little as 20 years after deglaciation (Egli et al., 2006). Chronosequence studies in proglacial areas have shown that within the initial 50 years, pioneer vegetation can establish dense cover (Conen et al., 2007), and mature vegetation (e.g., trees) can develop in less than 200 years (Crocker & Major, 1955). Nevertheless, a noticeable increase in organic matter (Crocker & Major, 1955; Egli et al., 2010) and a concurrent decrease in bulk density (He & Tang, 2008) can occur within the initial 200 years of soil formation. Glacier forefields are particularly well-suited for soil chronosequence studies, as the retreat of glaciers gives rise to a succession of moraines ranging from recently deglaciated areas to those that have been ice-free for thousands of years. This natural chronosequence allows exploring the rapid soil development that occurs on glacial till,

along with the evolution of vegetation and hydrological processes. Moreover, glacial forefields offer controlled settings with relatively consistent parent material and climate conditions, making it easier to isolate the effects of time on soil development and ecosystem dynamics. However, little is known about the effects on the hydrological response. While the evolution of the hillslope form (in terms of soil structure/properties and vegetation characteristics) in proglacial moraines has been previously studied (Crocker & Major, 1955; D'Amico et al., 2014; Douglass & Bockheim, 2006; Egli et al., 2010, 2012; He & Tang, 2008), the evolution of hillslope hydrological response related to the evolution of hillslope form during the first 10 millennia of landscape evolution has not been investigated in detail.

Our research aims to fill this knowledge gap by exploring the co-evolution of hillslope hydrological response and hillslope form during the initial 10 millennia of landscape evolution. Given the significant role of geology in catchment formation (Troch et al., 2015), we specifically investigate and compare the evolution of hillslope form and hydrological response in two contrasting geological settings. This research forms part of a larger collaborative endeavor involving hydrologists, geomorphologists, and geobotanists, focusing on two chronosequences of proglacial moraines. These moraines originate from siliceous and calcareous parent materials, each comprising four moraines aged from 30 to 13,500 years. The joint investigations on these moraines have yielded valuable insights into distinct aspects of hillslope form and hydrological response. The evolution of hillslope hydrological response was explored in terms of long-term changes in surface and subsurface runoff generation mechanisms (Maier & van Meerveld, 2021b; Maier et al., 2021) and the evolution of subsurface vertical flow paths (Hartmann, Semenova, et al., 2020; Hartmann et al., 2022). These publications also made initial attempts to correlate observed evolution with soil and vegetation changes. Regarding the evolution of form, the collaborative effort delved into the evolution of soil (hydraulic) properties (Hartmann, Weiler, & Blume, 2020a; Musso et al., 2019) and surface and subsurface vegetation characteristics (Greinwald, Dieckmann, et al., 2021; Greinwald, Gebauer, Musso, & Scherer-Lorenzen, 2021; Greinwald, Gebauer, Treuter, et al., 2021). Works by Musso et al. (2020, 2022b) provided detailed insights into soil erosion rates and soil formation, forming a comprehensive understanding of the evolving hillslopes.

Building upon the above listed publications, our study aims at synthesizing these findings with a focus on subsurface flow responses by also integrating analyses of soil moisture responses and deuterium soil water profiles in response to irrigation experiments. We defined hillslope form (mainly subsurface, surface, and vegetation characteristics, but not larger scale topography) and its evolution for each chronosequence by analyzing soil physical and hydraulic properties (texture and structure; Hartmann, Weiler, & Blume, 2020a). We also incorporated surface characteristics measured at the same sites by our collaborators (e.g., vegetation characteristics (Greinwald, Dieckmann, et al., 2021), hydrophobicity, and microtopography (Maier & van Meerveld, 2021b; Maier et al., 2021)). To assess the soil hydrologic response and its evolution over time, we examined soil moisture signatures, soil water isotope profiles, and the occurrence of preferential flow from tracer irrigation experiments. Our aim is to comprehensively examine the co-evolution of soil, vegetation, and water transport in both siliceous and calcareous materials by going beyond individual facets, synthesizing various aspects to unveil the detailed links between hillslope form and hydrological response evolution and their dependence on geological parent material. This synthesis represents a crucial expansion and deepening of the insights gained thus far, contributing substantially to the existing body of knowledge.

Moving beyond the aspect of landscape evolution, the identified links between hillslope form and hydrological functioning can be valuable for the initial assessment of landscape hydrology with limited monitoring data, allowing us to draw preliminary conclusions about the hydrological response based on easily measured or observed landscape properties. This effort contributes to the transfer of knowledge and process similarity, essential steps for the hydrological assessment of ungauged landscapes (Blöschl, 2016).

In summary, we compared the evolution of hillslope form and hydrological response in two contrasting geologies, that is, siliceous and calcareous parent materials. Specifically, we addressed three questions: (a) How do soil structural features and vegetation characteristics evolve in these materials? (b) How does the hydrological response differ between them? (c) Can we identify general links between form and functioning, regardless of age and parent material? Our study contributes to expanding the knowledge and data on how hydrologic processes depend on landscape structure and co-evolve within the hydro-pedogeomorphological system feedback cycle. Figure 1 provides a graphical overview of our research approach to address these questions.

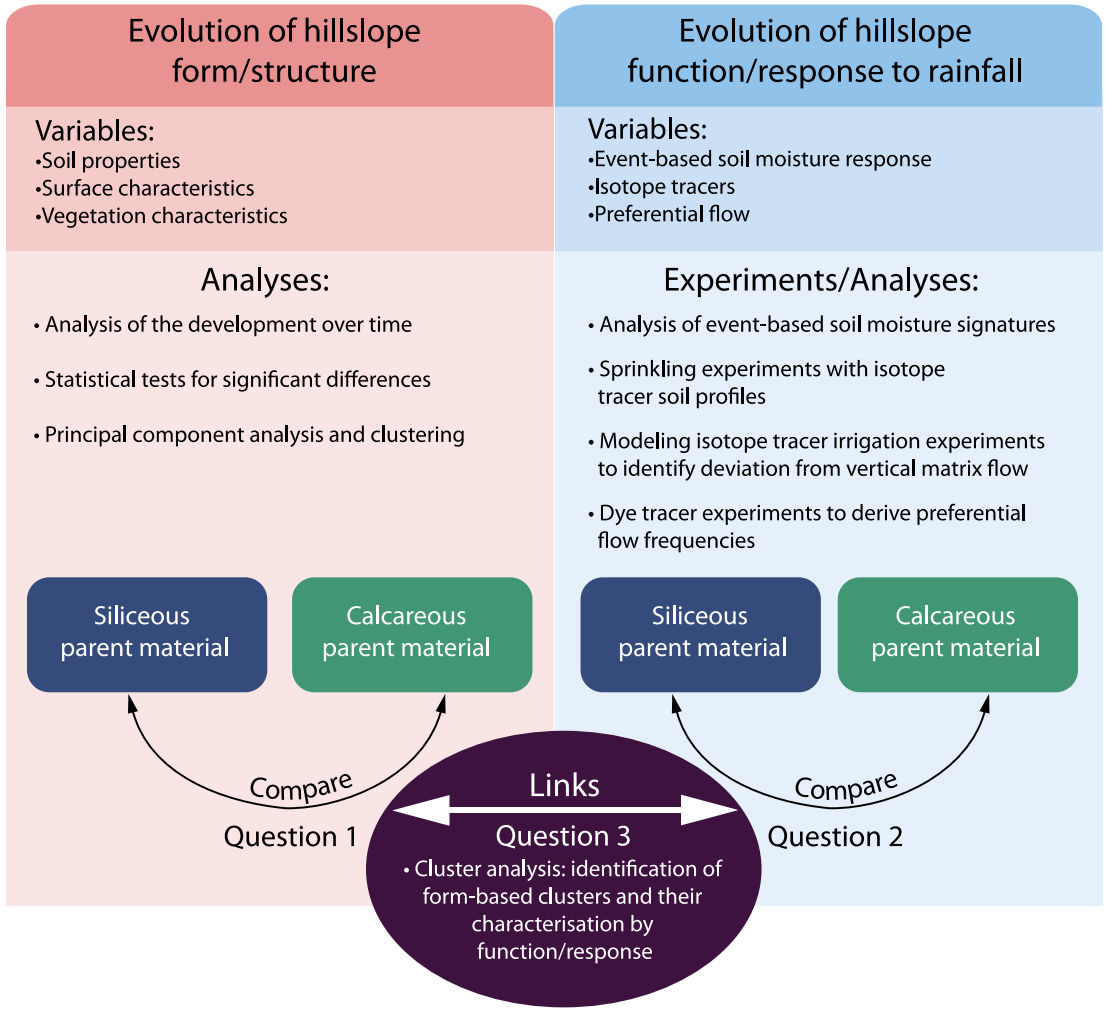

Figure 1. Summary of the research approach.

2. Material and Methods

2.1. Study Areas

We studied two chronosequences in two different glacier forefields in the Central Swiss Alps. Each chronosequence study was based on four moraines of different ages and included extensive sampling, surveying and irrigation experiments. The first chronosequence is located in the glacier forefield of the Stein Glacier, south of the Sustenpass in the Urner Alps (47° 43′N, 8° 25′E) at an elevation of 1,980 m.a.s.l. At this study area, the soils developed on siliceous glacial till. The second chronosequence is located in the glacier forefield of the Griessfirn, near the Klausenpass in the canton of Uri (appr. 46° 85′N, 8° 82′E). The study area is located at an elevation between 2,030 and 2,200 m a.s.l. Here, the soils developed on calcareous glacial till. The siliceous parent material (S-PM) consists mainly of metamorphosed pre-Mesozoic metagranitoids, gneisses, and amphibolites (Heikkinen & Fogelberg, 1980; Schimmelpfennig et al., 2014). The calcareous parent material (C-PM) is mainly limestone (Frey, 1965) deposited during the early Jurassic to Tertiary era (Musso et al., 2019). A detailed description of the parent material composition is provided by Musso et al. (2019, 2020).

The closest weather station to the S-PM forefield (distance: 18 km) is Grimsel Hospiz (46° 34′N, 8° 19′E) at an elevation of 1,980 m a.s.l. The recorded mean annual temperature is 1.9°C and the mean annual precipitation is 1,856 mm (1981–2010) (MeteoSwiss, 2020a). The closest weather station to the C-PM forefield (distance: 48 km) is Pilatus Mountain (46° 98′N, 8° 25′E) at an elevation of 2,106 m a.s.l. The recorded annual mean temperature is 1.8°C and the annual precipitation is 1,752 mm (1981–2010) (MeteoSwiss, 2020b).

At each glacier forefield, a moraine chronosequence of four different age classes was identified. Details on the dating of the moraine ages are provided by Musso et al. (2019). The four age classes at S-PM are 30 (30a; a = years), 160 (160a), 3,000 (3ka; k = 1,000), and 10,000 (10ka) years and at C-PM 110 (110a), 160 (160a), 4,900 (4.9ka), and 13,500 (13.5ka) years. The choice of the 110 year old moraine at C-PM as the youngest moraine is the result of the local conditions, as no adequate moraine with an age of around 30 years could be identified that also ensured comparability in terms of elevation and micro climate. Choosing the 110 years moraine as our youngest moraine at C-PM was therefore the best compromise.

The soils were classified according to the World Reference Base for Soil Resources (IUSS Working Group WRB, 2014; Maier et al., 2020; Musso et al., 2019, 2020). The soils at S-PM were classified as a Hyperskeletic Leptosol (30a, 160a), a Skeletic Cambisol (3ka), and Dystric Cambisol/Skeletic Cambisol/Entic Podzol (10ka). The soils at C-PM were classified as a Hperskeletic Leptosol (110a, 160a) and as a Calcaric Skeletic Cambisol (4.9ka, 13.5ka, Figure C1).

The vegetation cover at both forefields differs among the four age classes. At S-PM, the vegetation cover at 30a consists mainly of sparsely distributed grass, moss, forbs, and a few shrubs. The 160a and 3ka moraines are occasionally grazed by cows and sheep, which was prevented for the duration of the experiments by fencing in the study areas. The dominant vegetation types at the 160a moraine are grasses, lichen, forbs, and shrubs. The 3ka is mainly covered by grasses with fern, mosses, sedges and forbs. The oldest moraine is dominantly covered by a variety of prostrate shrubs, small trees and several grasses. At the C-PM, the vegetation cover at 110a and 160a is sparsely distributed with patches of grass and forbs at the 160a and patches of mostly mosses and lichens at the 110a. The two oldest moraines (13.5ka and 4.9ka) are both densely covered with grass, dwarf shrubs and sedge. Until a few years ago both moraines were occasionally used for grazing. More information on the vegetation cover composition and an analysis of their functional community structure at both forefields is provided by Greinwald, Gebauer, Musso, and Scherer-Lorenzen (2021).

Further information on vegetation and (soil) surface properties such as above ground biomass (BM), root length density (RLD), root density (RD), specific root length (SRL), vegetation surface coverage (SC) were determined by Greinwald, Dieckmann, et al. (2021) and saturated hydraulic conductivity (KS), surface hydrophobicity (HP), and microtopography (MT) were determined by Maier et al. (2020, 2021), and Maier and van Meerveld (2021b). All of this information was recorded for each of three areas of the moraines (identified as plots 1–3) that comprise the experimental plots used for the tracer experiments described in Section 2.2. Musso et al. (2019) measured soil-pH across the moraines in both forefields. The locations of the pH measurements differ slightly from the sampling locations of the other variables. Table 1 summarizes the gathered information, including details on slope and aspects previously reported by Musso et al. (2019, 2020) (Figure 2).

Considering that slope, aspect, and slope position can influence soil hydrological conditions, the aim was to select hillslopes with comparable characteristics. This was achieved for the majority of the slopes; however, due to specific site restrictions, there are also a few outliers with different slope, aspect (Table 1), or slope position. For the siliceous parent material, plot slopes range from 18° to 34°, with the majority falling between 20° and 30°. On the calcareous site, slopes range from 29° to 38°, with most between 33° and 35°. The majority of the study plots have a northward orientation (Table 1). Experimental plots and sampling locations were mainly on the backslope of hillslopes, except for the lower edge of irrigation plots 2 and 3 on the youngest siliceous moraine, positioned relatively close to the footslope. The sampling points, however, were located on the backslope. The dye tracer experimental plots were primarily located at the backslope of the hills, except for plot 3 on the 160-year-old moraine and plot 1 on the 13,500-year-old moraine in the calcareous forefield, which were both situated close to the rim (see Figures 3c and 3f). Considering periglacial processes like solifluction, which can potentially impact the evolution of soil and biota on periglacial moraines, we took special care in selecting moraines and plot positions where clear signs of such influences were minimal.

2.2. Soil Physical and Soil Hydraulic Properties Estimation

To describe the hillslope structure in terms of soil physical and hydraulic properties disturbed and undisturbed soil samples were taken in 10, 30, and 50 cm depth at the irrigation experiment plots next to the soil moisture sensor profile and 1 m upslope of the lower plot boundary. At the 110a moraine at C-PM, the samples were taken in the undisturbed parts of the dye tracer experiment plots. We determined soil texture (gravel, sand, silt, and clay

Table 1
Vegetation and (Soil) Surface Characteristics of the Four Moraines at the Siliceous and Calcareous Parent Material

Moraine age (years)	Plot #	Slope[a] (°)	Aspect[a]	SC	RLD[b]	RD[b]	SRL[b]	BM[b]	Ksat[b] (0–20 cm)	Ksat[c] (20–40 cm)	HP[c]	MT[c]	pH range[d,e] (mean)[d,e]
Siliceous parent material													
30a	1	34	NE	20	152.1	0.84	198.4	0.93	2,510.5	74.2	1.6	0.52	6.1–6.7 (6.5)
	2	23	NE	60	523.2	3.3	176.31	3.28	3,831.5	83	1.25	0.36	
	3	21	NE	50	250.9	1.5	152.1	5.1	2,505.3	176.4	0.82	0.55	
160a	1	31	NE	100	1,180.8	4.9	237.9	6.6	1,925.7	296.5	2.55	0.29	4.7–5.5 (4.9)
	2	26	NE	80	832.9	4.7	177.8	29.5	2,219.0	99.3	1.4	0.36	
	3	25	NE	60	798.7	5.1	188.6	3.2	1,240.4	301.3	1.9	0.29	
3ka	1	25	SE	70	918.4	9.5	102.2	10.1	582	128.6	3.3	0.33	4.6–6.1 (5.2)
	2	25	S	80	825.6	6.3	131.3	11.4	744.9	120.8	2.04	0.58	
	3	32	S	90	861.7	10.0	88.4	8.1	1,063.5	53.0	3.1	0.65	
10ka	1	26	N	90	304.7	4.4	66.3	50.9	787.1	7.0	2.5	1.14	3.4–4.4 (4.0)
	2	24	NE	80	463.6	3.7	122.1	23.9	219.8	16.7	9.1	0.64	
	3	18	NE	100	424.2	4.2	98.8	18.9	263.3	29.3	4.2	1.08	
Calcareous parent material													
110a	1	–	WNW	55	150.6	0.83	129.8	n.a.	n.a.	n.a.	n.a.	n.a.	7.6–7.8 (7.7)
	2	–	WNW	25	348.6	4.56	78.4	n.a.	n.a.	n.a.	n.a.	n.a.	
	3	–	WNW	15	315.13	1.36	222.4	n.a.	n.a.	n.a.	n.a.	n.a.	
160a	1	35	E	20	201.4	1.27	172.3	5.7	4,695.3	192.8	1.04	0.34	7.3–7.8 (7.6)
	2	29	NW	50	293.18	2.75	104.3	4.7	472.9	72.7	2.46	0.36	
	3	33	NE	75	165.9	2.97	58.1	3.9	1,877.2	272.1	1.8	0.27	
4.9ka	1	34	W	90	822.9	5.8	142.8	9.6	3,206.0	38.8	5.5	0.63	4.5–7.8 (6.9)
	2	28	SE	90	939.8	10.2	93.0	5.5	1,670.9	31.6	2.96	0.29	
	3	33	NE	100	1,235.16	7.8	161.4	8.7	1,124.5	40.9	6.73	0.26	
13.5ka	1	33	NE	85	654.2	9.5	68.34	4.9	799.4	23.9	7.72	0.3	5.9–7.8 (7.3)
	2	38	NE	80	608.7	6.0	111.8	4.6	813.9	29.9	5.9	0.25	
	3	35	NW	100	1,197.3	10.4	121.3	3.6	890.1	6.8	14.5	0.28	

[a]This information was compiled from Musso et al. (2019) and Maier et al. (2020). [b]This information was compiled from Greinwald, Dieckmann, et al. (2021) RLD = root length density (km m^{-3}), RD = root density (kg m^{-3}), SRL = specific root length (m g^{-1}), BM = above ground biomass (kg m^{-2}). [c]This information was compiled from Maier and van Meerveld (2021a) Ksat = saturated hydraulic conductivity (cm d^{-1}), HP = hdrophobicity [–], MT = microtopography [–]. [d]This information was compiled from Musso et al. (2022b) pH = pH-value [-] (range and mean). [e]The locations of the pH measurements differ from the sampling locations of the other variables.

content), porosity, bulk density, organic matter content, the soil water retention curves, and soil hydraulic conductivity curves. A detailed description of the methods and data differentiated by depth is provided in Hartmann, Weiler, and Blume (2020a). The data sets are available at Hartmann, Weiler, and Blume (2020b).

Based on the measured retention curves, the van-Genuchten parameters (Van Genuchten, 1980) required for soil water transport model parameterization were determined with the curve fitting function of the HYPROP-Fit software (Pertassek et al., 2015, METER Group, Inc. USA). Using the fitted curves, the available water capacity (AWC) was determined as the difference in water content between pF = 1.8 (field capacity) and pF = 4.2 (permanent wilting point) with $pF = \log_{10}(|\text{pressure head (cm)}|)$.

2.3. Tracer Experiments

To gain comprehensive insights into the hillslope hydrological response, we conducted two types of tracer experiments on each moraine. Dye tracer experiments were used to visualize vertical subsurface flow paths and to

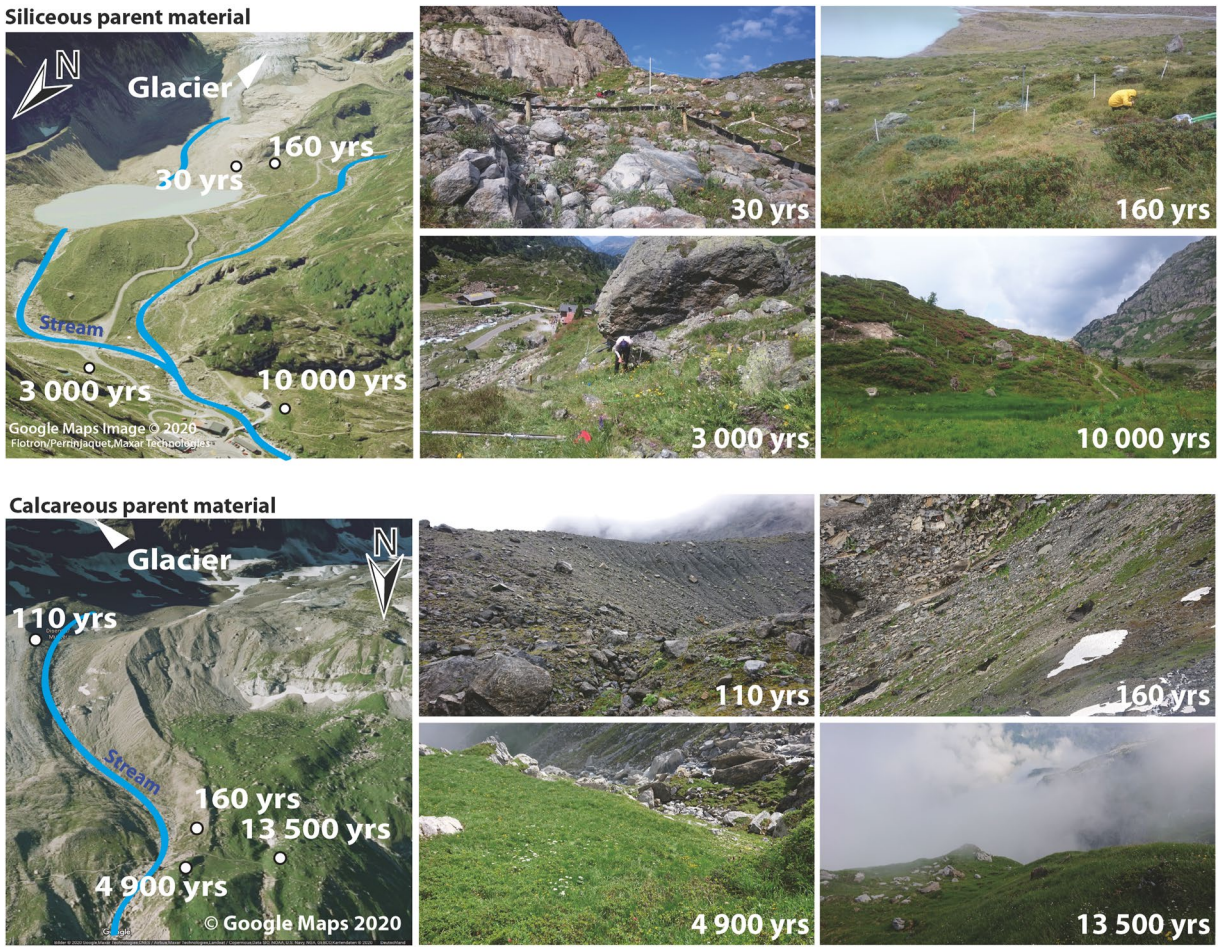

Figure 2. Glacier forefield and location of the four selected moraines of the siliceous parent material (S-PM, top (Google Maps, 2020b)) and the calcareous parent material (C-PM, bottomt (Google Maps, 2020a)). Figure adapted from (Hartmann, Weiler, & Blume, 2020a; Hartmann et al., 2022).

derive vertical subsurface flow types. Irrigation experiments on plots equipped with soil moisture sensors were used to draw conclusions about characteristic hillslope functions based on soil moisture signatures. The irrigated water was labeled with deuterium (δ^2H) and the subsequent analysis of δ^2H in the soil water profiles were used to derive dominating water flow components (e.g., surface runoff, lateral subsurface flow, vertical percolation including preferential flow). These experiments, conducted in direct vicinity to each other (Figure 3), present a multi-faceted approach to studying the hillslope hydrological response. Our analyses, conducted at both plot and larger plot scales, enable us to grasp the nuances of hydrological processes influencing hillslope behavior. These detailed, sub-meter scale observations act as crucial indicators, collectively improving our comprehension of broader hillslope hydrology.

2.3.1. Dye Tracer Experiments

The dye tracer experiments at the S-PM chronosequence were conducted between mid-July and mid-August 2018 and at C-PM between August and mid-September 2019. At each moraine, the experiments were carried out on three experimental plots (1 m × 1.5 m) differing in their vegetation complexity (Greinwald, Dieckmann, et al., 2021). The experimental setup and detailed analysis of the dye tracer experiments are described in detail in Hartmann, Semenova, et al. (2020) (S-PM) and Hartmann et al. (2022) (C-PM). Based on the resulting dye patterns a flow type frequency distribution was estimated using the classification method proposed by Weiler (2001) and modified by Hartmann, Semenova, et al. (2020). Five flow types were distinguished: (a) macropore flow with low interaction, (b) mixed macropore flow (low and high interaction), (c) macropore flow with high interaction/finger-like flow, (d) heterogeneous matrix flow/finger-like flow, and (e) homogeneous matrix flow (incl. between rocks). Dye patterns, which could not be classified as one of these flow types were

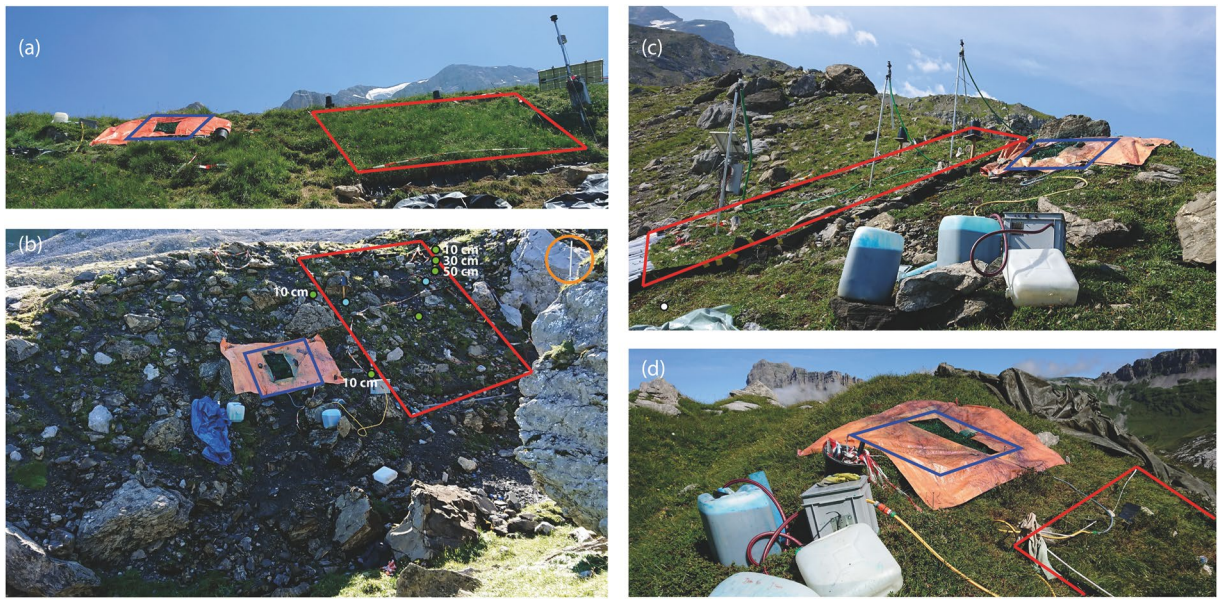

Figure 3. Examples for the positions of the dye tracer plots (blue rectangles) in relation to the isotope tracer plots (red rectangles) at three moraines at the C-PM forefield. Examples show experiments on the (a) 4.9ka, (b, c) 160a, and (d) 13.5ka moraine. (b) The positions of the soil moisture sensors (green dots), tipping bucket (turquoise dots), and weather station (orange circle).

categorized as undefined. A preferential flow fraction index (PFF, Hartmann et al., 2022) was calculated as the observed fraction of all preferential flow type classes (flow types a–d) at each profile. The flow type classification was done for each depth segment of the soil profile, with the size of a segment being 1 mm. PFF is the number of segments classified as a preferential flow type divided by the total number of segments per soil profile. PFF is calculated for each irrigation plot per age class (3), each subplot per plot (3), and for each number of photographs taken per subplot (5). This means that the maximum sample size of PFF values per age class is 45. However, sample size decreases if there are no observations of infiltrated water at the specified depths (10, 30, 50 cm) or if the number of photographs has been reduced due to local conditions (e.g., huge boulders, collapsing pits).

2.3.2. Isotope Tracer Experiments

The δ^2H-irrigation experiments were conducted on three plots (4 m × 6 m) per moraine between mid-July and September 2018 at S-PM and in August 2019 at the C-PM chronosequence. The 110a moraine at C-PM was excluded due to its difficult access. The irrigation plots were chosen along a vegetation complexity gradient (Greinwald, Dieckmann, et al., 2021). Each plot was equipped with 6 soil moisture sensors (SMT100, TRUEBNER GmbH, Germany). A sensor profile with sensors in 10, 30, and 50 cm depth was installed at one side of the plot about 1 m downslope from the upper plot boundary. On the other side of the plot, two sensors were placed in 10 cm depth, one opposite to the sensor profile and the second sensor 1 m upslope from the lower plot boundary. The sixth sensor was placed at 10 cm depth in the center of the plot (Figure 3). Two tipping bucket rain gauges per plot were installed for the monitoring of the irrigation experiments and natural rainfall events. Weather stations consisting of an extra tipping bucket, two solar radiation sensors (CS 305-ET, Campbell Scientific, Inc.) for measuring the incoming and reflected short wave radiation (300–1,000 nm), a 2-D sonic wind sensor (WindSonic, Campbell Scientific, Inc.) for measuring wind speed and direction, as well as an air temperature and relative humidity sensor were installed at the 10ka, 3ka, and 30a moraine at the S-PM and at the 4.9ka and 13.5ka at the C-PM forefield. All data were recorded at a 1 minute resolution. Trenches were installed to record surface and subsurface flow. A detailed description of the surface runoff and subsurface flow measurements at the trenches and an evaluation of the results is provided by Maier et al. (2021) and Maier and van Meerveld (2021b). In contrast, here we are looking only at the soil water reaction and soil water isotope profiles.

The plots were irrigated on three consecutive days with three different irrigation intensities and δ^2H-concentrations. The irrigation intensity was increased step-wise every day while the isotope concentration was decreased. A detailed overview of the irrigation intensities and δ^2H-concentrations per plot, age class, and parent material is

given in Table 2. Soil profile samples for the isotope analysis were collected at each plot in 10 cm depth increments from a soil core of 8 cm diameter, excavated with a percussion drill a few days before the irrigation experiments (Background samples), two days after the last irrigation experiment (Profile 1 samples), and 5–14 days after the last irrigation experiment (Profile 2 samples). The variation in the sampling time of the second profile is due to logistical reasons. The isotopic composition of the soil water was analyzed according to the equilibration method (Wassenaar et al., 2008). Soil samples were stored in airtight bags filled with dry air and sealed by welding. The samples were stored for 48 hr for equilibrium at a low temperature and then analyzed. In addition to the soil samples, three standard bags were prepared in the same manner containing 10 ml of water with a known δ^2H-concentration (−126.07, −67.27, −2.57 ‰), which were then handled the same as the soil samples. The isotopic composition in the headspace of the sample bags was measured with a wavelength-scanned cavity ring-down spectrometer (L2130-i, Picarro). The air was extracted from the bag into the spectrometer by inserting a needle into the bag via a previously attached silicone septum and connecting PVC tubing. A measurement was taken as the average over a 90 s period, when the standard deviation for H2O was below 100 ppm, for δ^{18}O below 0.6 ‰, and for δ^2H below 1.2 ‰. The standard bags were measured before and after the soil samples to transform the measurements into the δ-notation relative to the Vienna Standard Mean Ocean Water (VSMOW) and to account for any temperature related drift. The data was corrected according to Gralher et al. (2016) to account for the potential risk of CO_2 formation during the equilibration caused by organic material and soil bacteria. Water samples of the irrigation water enriched with δ^2H were sampled from the storage basins directly before the experiment and were analyzed with a similar wavelength-scanned cavity ring-down spectrometer (L2130-i, Picarro, Inc.) in the Stable Isotope Lab at Freiburg University.

2.4. Modeling of Soil Water Isotope Profiles

To infer dominant water flow processes based on one-dimensional δ^2H-profile information, we used the approach proposed by Müller et al. (2014). The approach is based on the assumption that characteristic deviations between δ^2H-profiles modeled only by vertical matrix flow and measured δ^2H-profiles, provide conclusions about dominating flow components such as lateral subsurface flow and vertical percolation including preferential flow. The soil water isotope profiles were modeled by using the modified version (Stumpp et al., 2012) of the HYDRUS-1D software package (Šimůnek et al., 2016). This model calculates the transient water flow by numerically solving the Richards equation and the isotope transport with the advection–dispersion model. The model does not account for fractionation processes during evaporation that can lead to an isotopic enrichment of the soil.

Each irrigation experiment plot was modeled individually by parameterizing a 150 cm deep soil profile. The estimated van Genuchten parameters based on the measured water retention curves and measured saturated hydraulic conductivities (Maier et al., 2020) were used to parameterize the Richards equation. Since van Genuchten parameters were available in 10, 30, and 50 cm depth, the model domain was subdivided into three materials (material 1: 0–20, material 2: 20–40, and material 3: 40–150 cm). At depths with two measured retention curves, a parameter set describing the mean retention curve was used. This was done by averaging the parameters and double checking visually if the resulting retention function can be considered the mean of these functions.

The modeling period extends from the day the background δ^2H-profile was sampled to the day the second δ^2H-profile was taken after the last irrigation experiment. The period between the background sampling and the first irrigation experiments is specifically designated as the ”spin-up phase” where the model is getting acclimated under natural rainfall conditions. The mean values from both rain gauges per plot were used as the precipitation input. For the atmospheric boundary conditions we calculated the daily potential evapotranspiration using the FAO-Penman-Monteith method (Allen et al., 1998) based on the measured information on temperature, wind speed, humidity, and incoming and reflected shortwave radiation. The potential evaporation functions as a flux boundary condition until a critical pressure head is achieved. Once this threshold is reached, the threshold value is used as a pressure head boundary condition and the actual evaporation flux is calculated using the Richards equation. The potential transpiration is adjusted to actual transpiration (root water uptake) based on the extractable water availability in the root zone. The depth dependent water extraction due to root water uptake was specified by measured root length density distributions down to a depth of 1 m provided by Greinwald, Dieckmann, et al. (2021), which were measured in the same soil samples used for the soil water isotopic analysis. The initial pressure head conditions for the water transport were set to field capacity and the initial distribution of the δ^2H-concentration was specified by using the background profile information

Water Resources Research

10.1029/2023WR035937

Table 2
Irrigation Amount, Irrigation Intensity and δ^2H-Concentration of the Irrigated Water During the 3-Day Irrigation Experiments at all Three Irrigation Plots per Age Class at the S-PM and C-PM Forefield

	Irrigation			Irrigation			Irrigation		
	Day 1			Day 2			Day 3		
Plot 1	Amount (mm)	Intensity (mm h^{-1})	δ^2H (‰)	Amount (mm)	Intensity (mm h^{-1})	δ^2H (‰)	Amount (mm)	Intensity (mm h^{-1})	δ^2H (‰)
Moraine									
Siliceous parent material									
30a	21	23	51.05	33	54	−11.30	36	61	−61.11
160a	23	22	76.72	52	56	10.13	63	90	−56.05
3ka	16	14	95.16	44	63	45.25	35	67	−61.66
10ka	12	13	242.41	27	26	26.57	19	33	−53.12
Calcareous parent material									
160a	27	26	205.90	60	61	130.25	70	79	71.29
4.9ka	26	24	230.37	45	49	128.86	41	77	81.20
13.5ka	25	22	240.42	31	32	143.09	51	56	79.76

	Irrigation			Irrigation			Irrigation		
	day 1			day 2			day 3		
Plot 2	Amount (mm)	Intensity (mm h^{-1})	δ^2H (‰)	Amount (mm)	Intensity (mm h^{-1})	δ^2H (‰)	Amount (mm)	Intensity (mm h^{-1})	δ^2H (‰)
Moraine									
Siliceous parent material									
30a	18	14	49.42	27	33	−11.02	27	46	−58.85
160a	20	23	85.69	32	40	5.17	54	62	−53.32
3ka	14	11	92.97	24	32	5.31	31	43	−54.10
10ka	12	13	242.48	22	24	12.19	24	43	−60.69
Calcareous parent material									
160a	26	24	233.04	47	50	124.61	42	63	72.18
4.9ka	22	23	209.28	37	45	152.44	46	79	99.81
13.5ka	25	23	257.99	35	35	118.66	48	72	72.57

	Irrigation			Irrigation			Irrigation		
	day 1			day 2			day 3		
Plot 3	Amount (mm)	Intensity (mm h^{-1})	δ^2H (‰)	Amount (mm)	Intensity (mm h^{-1})	δ^2H (‰)	Amount (mm)	Intensity (mm h^{-1})	δ^2H (‰)
Moraine									
Siliceous parent material									
30a	19	15	63.26	30	37	−3.62	32	48	−57.44
160a	23	20	73.77	25	43	6.53	57	81	−64.57
3ka	19	16	85.15	29	31	6.43	31	44	−54.25

Table 2
Continued

Plot 3	Irrigation day 1 Amount (mm)	Irrigation day 1 Intensity (mm h^{-1})	Irrigation day 1 δ^2H (‰)	Irrigation day 2 Amount (mm)	Irrigation day 2 Intensity (mm h^{-1})	Irrigation day 2 δ^2H (‰)	Irrigation day 3 Amount (mm)	Irrigation day 3 Intensity (mm h^{-1})	Irrigation day 3 δ^2H (‰)
10ka	10	11	236.79	17	23	18.51	18	32	−53.12
Calcareous parent material									
160a	22	24	264.48	53	58	123.37	53	70	73.91
4.9ka	25	23	232.14	38	44	121.92	51	61	74.53
13.5ka	26	24	244.28	45	59	96.41	52	78	69.56

(sampled before irrigation). δ^2H-concentration of the natural rainfall was either specified by laboratory measurements of occasional rainfall events or by monthly mean values from the GNIP station Grimsel (IAEA/WMO, 2021) which is located in a distance of 20 km to S-PM and 50 km to C-PM at an elevation of 1,950 m.a.s.l. The δ^2H-notation describes the divergence of the isotopic composition of a sample in relation to the VSMOW. Natural waters contain mostly less heavy isotopes than the VSMOW, which leads to negative δ^2H values. Due to our step-wise enrichment of the irrigation water, δ^2H-values range from negative to positive values. To calculate the δ^2H-transport with non-negative values, an offset of 120 was added to the input isotopic concentrations. The longitudinal dispersivity (D_L), a transport parameter in the advection–dispersion model, was unknown and had to be determined by manual calibration. For simplicity, D_L was assumed to be constant with depth. Each model was executed with seven different values for D_L (0.1, 0.5, 1, 1.5, 3, 5, 10, and 15 cm). The best fit D_L was identified visually by comparing model output isotope profiles to measured isotope profiles (Figures B1 and B2).

2.5. Soil Moisture Response Analysis

The hillslope hydrological functions such as generation of overland flow, vertical percolation, water storage, etc. are largely determined by the soil hydrological response. For an inter-comparison of the soil hydrological responses, we used soil moisture signatures describing the soil moisture reaction to each event of the δ^2H-irrigation experiments. Five soil moisture signatures (Figure 4 and Table 3) were used to describe the soil water dynamics in terms of velocity, timing, and magnitude. The soil moisture signatures were calculated per event for each plot using data from all five soil water sensors (three at 10 cm, one at 30 cm, and one at 50 cm depth). The event response time (RT) reflects the velocity of the first soil water response and is thus a characteristic of the effective soil hydraulic conductivity. It is defined as the number of minutes between the start of irrigation and the first soil moisture response. This was defined as the point in time when the soil moisture increase was larger than 0.04 cm^3 cm^{-3}, thus increasing above the noise range of the sensors.

The relative peak timing (PT) provides information on the balance between infiltration and drainage. This signature is defined as the time between the end of irrigation and Θ_{peak}. Θ_{peak} is defined as the maximum water content during the event period, which is the period from the start of irrigation to 3 hr after the end of irrigation. Negative values indicate that Θ_{peak} was reached before the end of irrigation, which can be caused either by saturation or a balance between infiltration and drainage during irrigation (steady state). To differentiate if the cases of PT < 0 are caused by saturation or by steady state soil moisture conditions during irrigation, we calculated the available remaining storage at peak soil moisture (PS, available peak storage) based on the difference between the saturated water content (Θ_{sat}) and Θ_{peak}. PS values close to 0 indicate that the soil moisture peak was reached due to saturation. An available storage distinctly greater than 0 indicates the occurrence of steady state flow.

The magnitude of the soil water response can be derived based on the soil moisture peak amplitude. We calculated the relative maximum storage increase (SI) by relating the difference between the soil moisture Θ_{peak} and Θ_{init} (response amplitude, Branger and McMillan (2020)) to the irrigation amount (I) in mm. To convert the moisture response amplitude from m^3/m^3 to mm, the response amplitude was multiplied by the depth increment represented by the sensor readings (20 cm). SI thus provides information on how much of the irrigation water filled up the short term storage in the soil (either directly or by displacing old water). To evaluate a post-event storage increase (ES), we related the difference between the water content 3 hr after the end of irrigation and Θ_{init} converted to mm to the irrigation amount. This parameter provides information on how much of the irrigated water (directly or by displacement) the soil can still hold 3 hr after the end of irrigation. The comparison of both signatures provides insights on the storage properties of the soil. The smaller the differences between SI and ES, the higher the water holding capacity of the soil. High SI-values, but low ES-values, on the other hand, indicate a low storage capacity and a fast subsurface water transport.

The signatures used for the soil water response depend on antecedent soil moisture. As the irrigation experiments were conducted in both forefields during the summer under nearly identical climatic conditions and in a relatively short time span to ensure uniform weather conditions, we consider antecedent

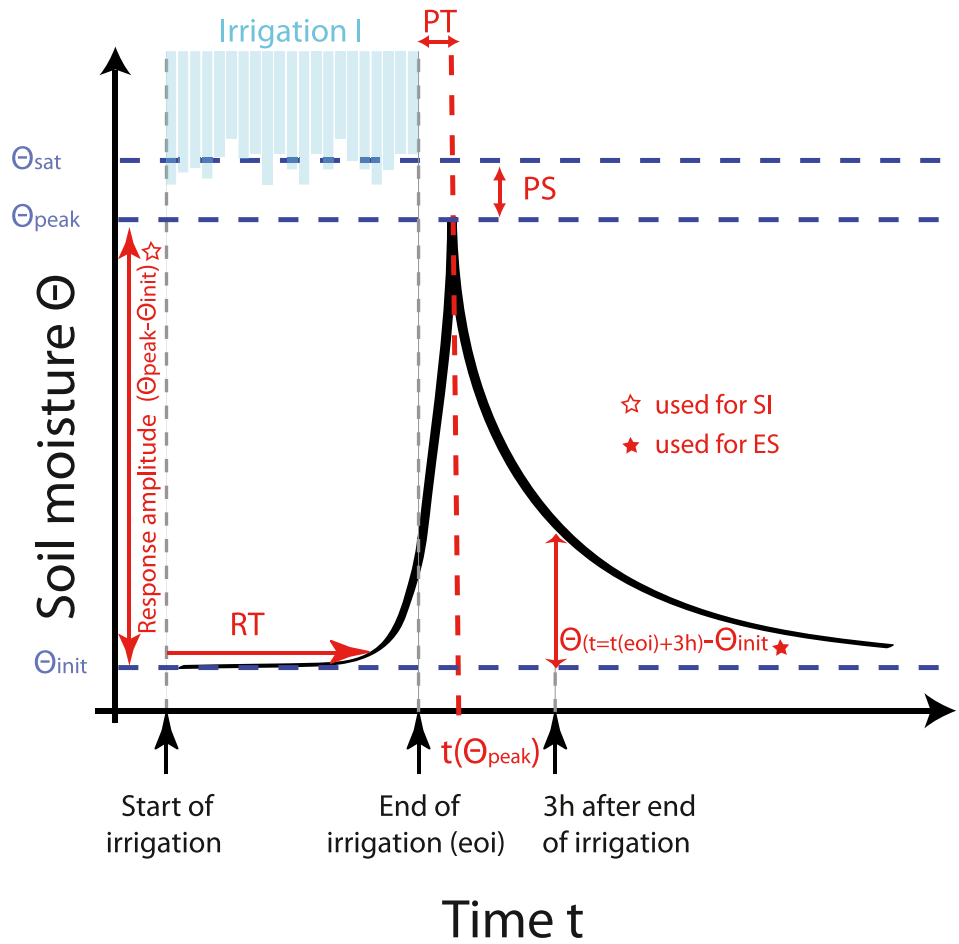

Figure 4. Visualization of the event-based soil moisture signatures listed in Table 3.

soil moisture as an intrinsic property defined by the underlying soil properties and thus characteristic for the individual age classes.

2.6. Statistical Analysis

The statistical analysis was carried out using R (R Core Team, 2017). The Mood's median test (Hervé, 2018) and the pairwise Mood's median post hoc test (Mangiafico, 2016) were used to test for significant differences in the

Table 3
Event-Based Soil Moisture Signatures and Their Calculation

Soil moisture signature [unit]	Abbreviation	Calculation	Description
Event response time [min]	RT	$t(\Theta - \Theta_{init} > 0.04)$	Velocity of soil water response,
Relative peak timing [min]	PT	$t(\Theta_{peak})$-t(end of irrigation)	Balance between infiltration and drainage
Available peak storage $\left[\frac{cm^3}{cm^3}\right]$	PS	$\Theta_{sat} - \Theta_{peak}$	Balance between infiltration and drainage
Relative maximum storage increase [%]	SI	$\frac{(\Theta_{peak} - \Theta_{init}) * 200[mm]}{I[mm]} * 100\%$	Magnitude of soil water response, maximum storage change
Relative event storage increase [%]	ES	$\frac{(\Theta_{3h\ after\ end\ of\ irrigation} - \Theta_{init}) * 200[mm]}{I[mm]} * 100\%$	Magnitude of soil water response, Differences to SI: information on storage capacity

Table 4
Abbreviations and Units of Soil, Vegetation, and Surface Characteristics Used in the Principle Component and Cluster Analysis

Characteristic	Abbreviation	Unit
Sand content	Snd	Weight (%)
Silt content	Slt	Weight (%)
Clay content	Cly	Weight (%)
Porosity	PO	$cm^3\ cm^{-3}$
Bulk density	BD	$g\ cm^{-3}$
Available Water Capacity	AWC	vol (%)
Sat. hydraulic conductivity	Ksat	$cm\ d^{-1}$
Above ground biomass	BM	$kg\ m^{-2}$
Organic matter content	OM	weight-%
Hydrophobicity	HP	[–]
Microtopography	MT	[–]
Vegetation surface coverage	SC	%
Root length density	RLD	$km\ m^{-3}$
Root density	RD	$kg\ m^{-3}$
Specific root length	SRL	$m\ g^{-1}$

observed soil-, surface-, and vegetation characteristics between the geologies and age classes. We tested for differences in the medians, as the median is less affected by outliers. The Mood's median test is a non-parametric test that compares median pairs of two or more groups. The significance level was set to $p < 0.05$.

A kmeans clustering and a principal component analysis using the prcomp-function was applied to the data describing hillslope form consisting of the soil property data in the top 10 cm and vegetation/surface characteristics. The analysis was limited to this depth because, for a subset of properties considered in this study, data availability is restricted to this specific depth. The 110a moraine at C-PM was excluded from this analysis due to missing data. To test for significant differences in the preferential flow fractions (PFF) and soil moisture signatures describing the hillslope response among the four clusters identified by kmeans, the Tukey's HSD (Honestly Significant Difference) test was used. The significance level was set to $p < 0.05$. The abbreviations and units of the soil-, surface-, and vegetation characteristics are listed in Table 4.

3. Results

3.1. Evolution of Hillslope Form

3.1.1. Evolution of Soil Characteristics

Figure 5 illustrates the evolution of soil properties presented as median values at depths of 10–50 cm, 10 cm, 30 cm, and 50 cm for the two geologies. Figure 6 shows the results of the Mood's median test for differences in soil properties between the age classes per geology (a) and between the geologies per age class (b). For the particle sizes at a depth of 10 cm at the 10ka moraine (Figures 6b-6 to 6b-8), a visual assessment of the differences was necessary because the sample size is significantly smaller than for the other age classes and geology ($n = 2$, instead of 6), which would produce misleading results in the Mood's median test.

The two geologies differ significantly in their soil structure (Figure 6b). At both geologies, we observed a decrease in sand content over time (Figure 5a). At the young age classes, the sand content at both geologies is high and differences between the geologies are small (110/30a, Figure 5) or not significant (160a, Figure 6b-5). With increasing age, the sand content on the calcareous parent material decreases significantly (Figures 5a and 6a-5). This is particularly pronounced at the depths of 10 and 30 cm. At the siliceous site, the sand content also decreases with age, but not as significantly. The content drops from roughly 70%–15% at the calcareous site and from approximately 80%–50% at the siliceous site. The silt content of both geologies shows no significant differences for the two young age classes (Figure 6b-6). On the calcareous parent material, the silt content increases significantly with age (Figure 6a-6), especially at the depths of 10 and 30 cm. The calcareous parent material has a significant higher clay content at all age classes compared to the siliceous parent material, but no clear age trend can be seen at either location.

Differences between the geologies in the development of bulk density and porosity are only significant at the medium age classes (160a and 3ka/4.9ka, Figures 6b-1 and 6b-2). A distinct decrease in bulk density with an associated distinct increase in porosity is observed at both geologies. While on the siliceous parent material, the bulk density and porosity differ significantly at all four age classes, the differences between the two oldest age classes on the calcareous parent material are not significant (Figures 6a-1 and 6a-2). Bulk density and porosity continuously develop in one direction (decrease in bulk density, increase in porosity) on the siliceous parent material, whereas on the calcareous parent material the differences between the oldest age classes are very small with the tendency to show a discontinuous development (extrema at 4.9ka instead of 13.5ka). The organic matter content increases with age on the siliceous parent material (Figure 6b-3) and is particularly high in the upper 10 cm at the oldest moraine. On the calcareous parent material, the organic matter also increases with age (Figure 5g) and is significantly higher at the age classes from 110 to 4.9k years compared to the siliceous parent material. At the oldest moraine of 10k years, the organic matter content of the siliceous parent material at 10 cm

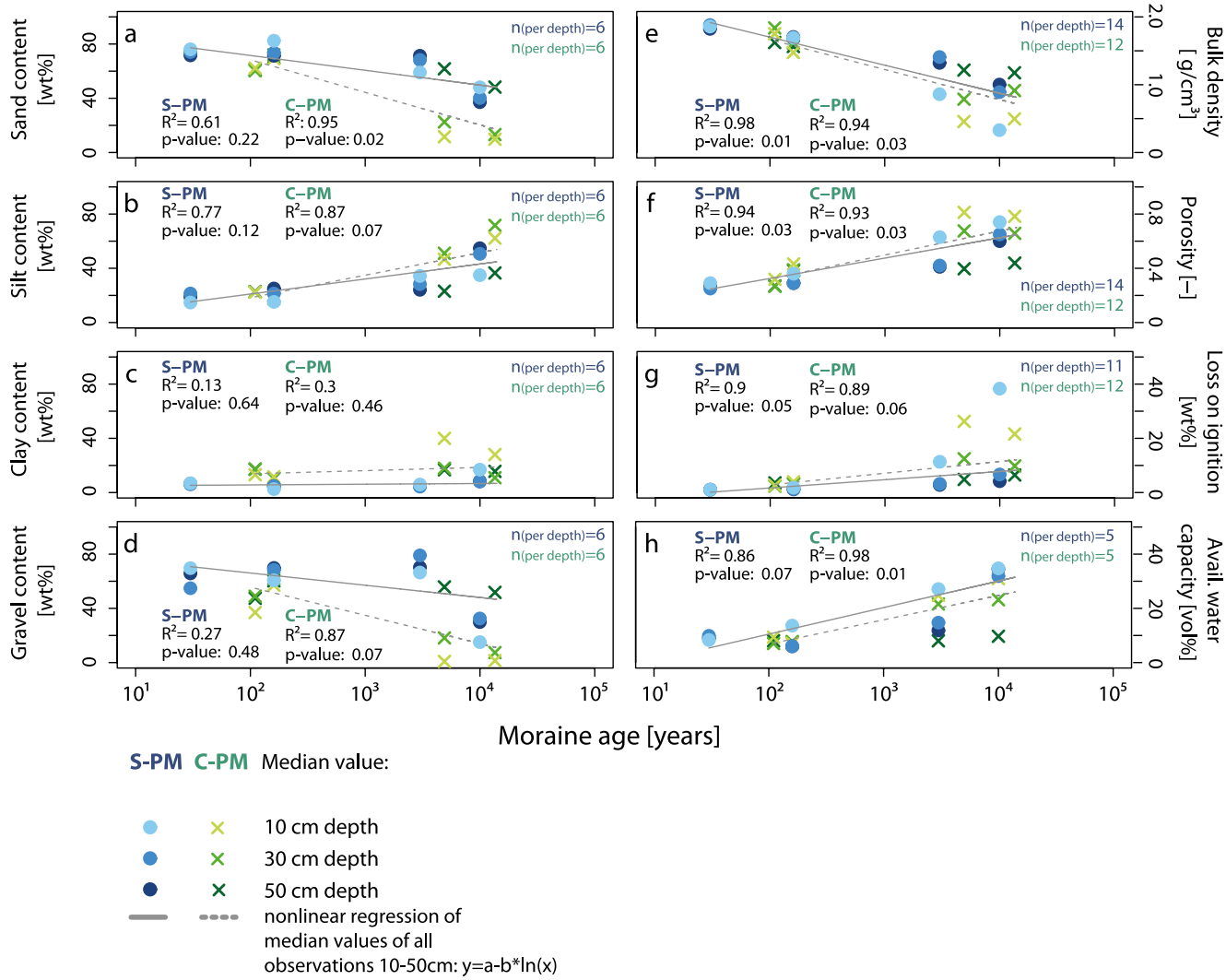

Figure 5. Evolution of median values of bulk density, porosity, loss on ignition, and sand, silt, and clay content at the siliceous (S-PM) and calcareous (C-PM) parent material for each age class in 10, 30, and 50 cm depth. The non-linear regression shows the age trend of the median of all values in 10–50 cm depth. *n* denotes the number of observations per depth and age class. Note that at the 10ka at S-PM at 10 cm depth n is only 2 for the observations of the sand, silt, clay, and gravel content.

depth exceeds that of the calcareous parent material (Figure 5g). The available water capacity increases with age at both geologies (Figure 5h). On the siliceous parent material, this increase is particularly distinct in the upper 10 cm up to an age of 3,000 years. At 10k years, the available water capacity in 30 and 50 cm depth varies in a similarly high range as in 10 cm depth. At the calcareous site, the available water capacity increases equally at 10 and 30 cm depth, with the highest values being reached at a depth of 10 cm. At a depth of 50 cm, on the other hand, the increase is only very slight, which leads to a large difference between the available water capacity in 10 and 50 cm depth.

Comparing both geologies, the most significant differences across all soil properties are found for the second oldest moraines (3k/4.9ka, Figure 6b). In the calcareous parent material, we observed a discontinuity in the age trend along the chronosequence with higher values in porosity, clay content, organic matter content, and lower values in bulk density at this age class compared to the oldest age class.

3.1.2. Cluster Analysis Based on Form

The following analysis delves into the outcomes of k-means clustering applied to soil, vegetation, and surface characteristics, identifying distinct patterns across the four identified clusters. To identify similarities and differences in form across age classes and between the two parent materials, we first conducted a principal component

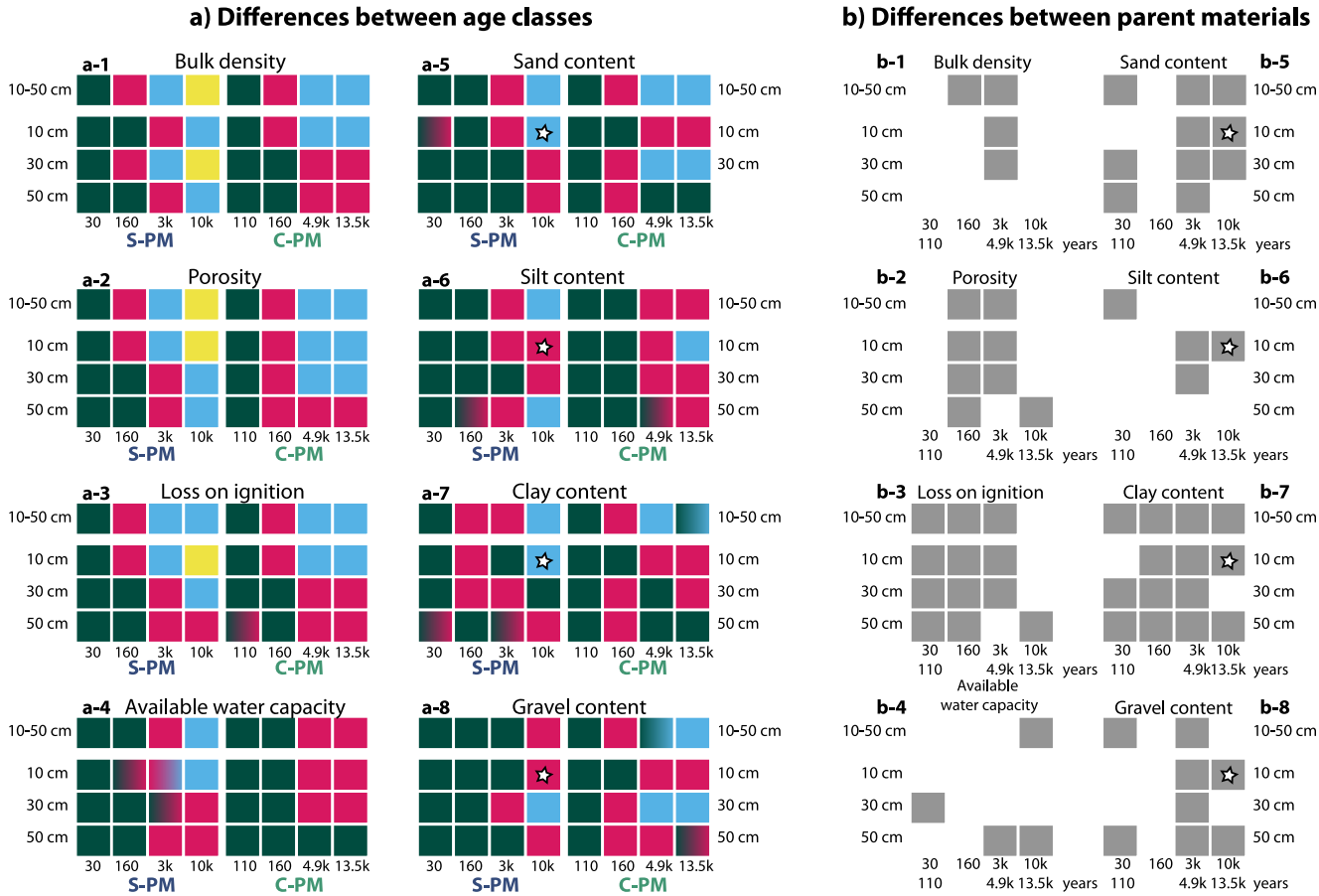

Figure 6. (a) Results of the Mood's median test conducted to identify significant differences between age classes for each parent material in soil properties at 10–50 cm, 10 cm, 30 cm, and 50 cm depths. Different colors represent significant differences between age classes. Age classes with the same color are not significantly different, as determined by the Mood's median test at the 0.05 level of significance. Partial coloring indicates a difference that is close to being significant. (b) Mood's median test to assess significant differences in soil properties at 10–50 cm, 10 cm, 30 cm, and 50 cm depths between parent materials for each age class and depth. Gray boxes indicate a significant difference between parent materials. A white star denotes visual evaluation of the differences. Visual assessment was necessary due to significantly different sample sizes, which could lead to misleading results in the Mood's median test. Please note that this test was not applied to identify differences between the different depths. To discern the direction of the difference, the reader is referred to Figure 5.

analysis on the set of form variables, which includes soil surface properties, surface characteristics, and vegetation characteristics. Subsequently, a cluster analysis was performed based on the results of the principal component analysis. The data on pH could not be included in the analysis due to an incompatibility of sampling locations and sampling strategy. However, because of its great importance, the influence of pH will be included in the discussion later on.

The principal component analysis of the combined set of form-describing data at S-PM and C-PM comprising soil properties in 10 cm depth and surface/vegetation characteristics (Table 1) shows that 70% of the variation in the data across the plots can be explained by the first two principal components (Figure 7). Soil properties such as porosity, bulk density, sand content, and available water capacity have the highest impact on the data distribution along the PC1 axis. Along the PC2 axis, microtopography and vegetation properties such as biomass, root length density and organic matter content have the highest impact.

We used k-means clustering to categorize the plots based on soil properties and surface characteristics represented in the first two principal components (PC1 and PC2). Among the four identified clusters, three predominantly align with the PC1 axis. Cluster 1, located on the far left of PC1 (Figure 7), includes the young moraines of both parent materials (30a + 160a S-PM and 160a C-PM) and is characterized by a high sand content and bulk density. Cluster 2, in the top right quadrant, comprises exclusively old moraines of C-PM (4.9ka + 13.5ka) and is distinguished by low sand content, high silt and clay content, high root density, root length density, and

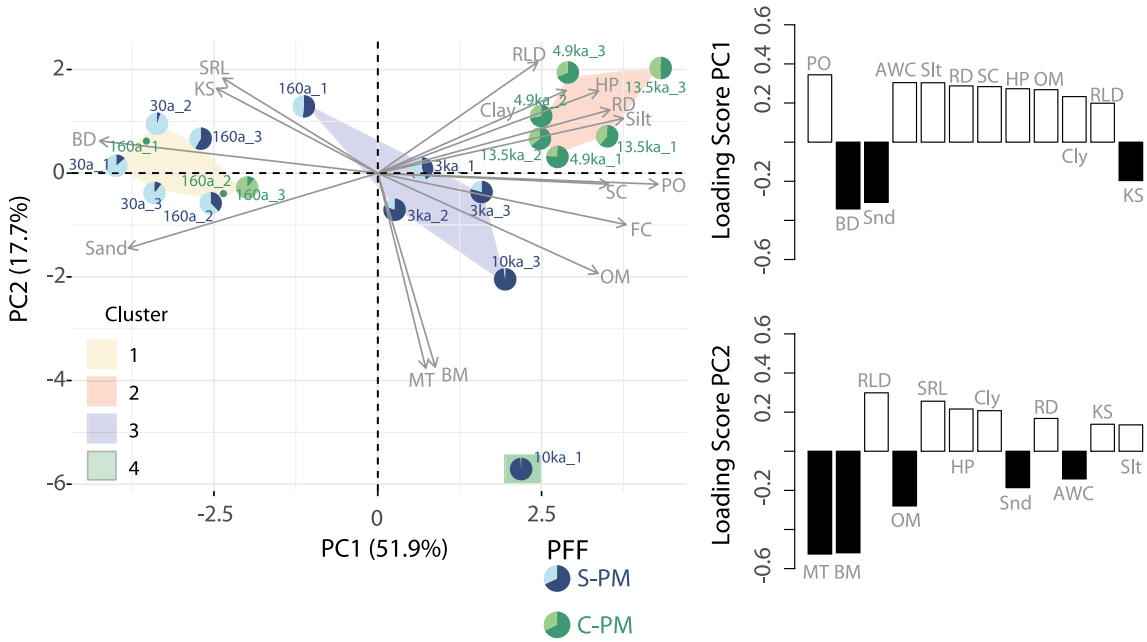

Figure 7. Left: Principal component analysis of data sets of S-PM and C-PM including soil properties at 10 cm depth and surface/vegetation characteristics data at each experiment plot per moraine with kmeans clustering. Pie charts show the corresponding preferential flow fraction (PFF) in the respective darker color. Right: The loading scores of the soil properties in 10 cm depth and surface/vegetation characteristics. Loading scores describe how much each variable contributes to PC1 and PC2. White indicates positive and black indicates negative loading scores. An explanation of the abbreviations is given in Table 4.

hydrophobicity. Cluster 3, positioned near the origin and extending along both directions of PC2, consists solely of moraines from S-PM. It encompasses all three plots from the 3ka, one from the 10ka, and one from the 160a moraine, exhibiting variations in saturated hydraulic conductivity, specific root length, and organic matter. The plot from the young moraine (160a) is located in the positive PC2 segment, displaying higher saturated hydraulic conductivity, specific root length, and lower organic matter and above-ground biomass. The fourth cluster, represented by a single plot from the 10ka moraine at S-PM, occupies a unique position primarily due to its high above-ground biomass, organic matter, and microtopography. In summary Cluster 1 features plots with coarse texture, low vegetation cover, and a weakly developed root system. In contrast, Cluster 2 is defined by finer material and a well-developed root system. Cluster 3 falls between these two, marked by higher above-ground biomass and pronounced microtopography. Cluster 4 stands out with the highest organic matter content, above-ground biomass, and available water holding capacity.

3.2. Evolution of Hillslope Function

3.2.1. Modeling Isotope Tracer Irrigation Experiments to Identify Deviations From Vertical Matrix Flow

We use the deviations between measured soil water δ^2H-profiles and modeled δ^2H-profiles (modeled by purely assuming vertical matrix flow) to infer dominant water flow processes as proposed by Müller et al. (2014). For simplicity, the longitudinal dispersivity D_L (Table B1) was assumed to be constant with depth. Both the measured and the modeled profiles of the δ^2H-concentration in the soil water 2 and 5–14 days after the third irrigation are shown in Figure 8. In the analysis, the model poorly reproduces soil profiles at both S-PM and C-PM. The observed differences suggest groundwater influence at the 30a moraine at S-PM and indicate preferential water transport in the other age classes at both S-PM and C-PM.

For S-PM, the model effectively reproduces the profiles of Plot 1 at the 30a moraine and the upper 60 cm of the three plots at the 160a moraine. Groundwater influence is evident in the other two plots at the 30a moraine, discerned from homogeneous isotopic concentrations in the lower part of the soil profile (Müller et al., 2014) and observations of saturated conditions during soil sampling with the percussion drill. This allowed an approximation of groundwater levels (GWL1 and GWL2 in Figure 8) for the days of sampling. Groundwater influence was further confirmed by observations of lateral subsurface flow (Maier et al., 2021). The proximity to the glacial

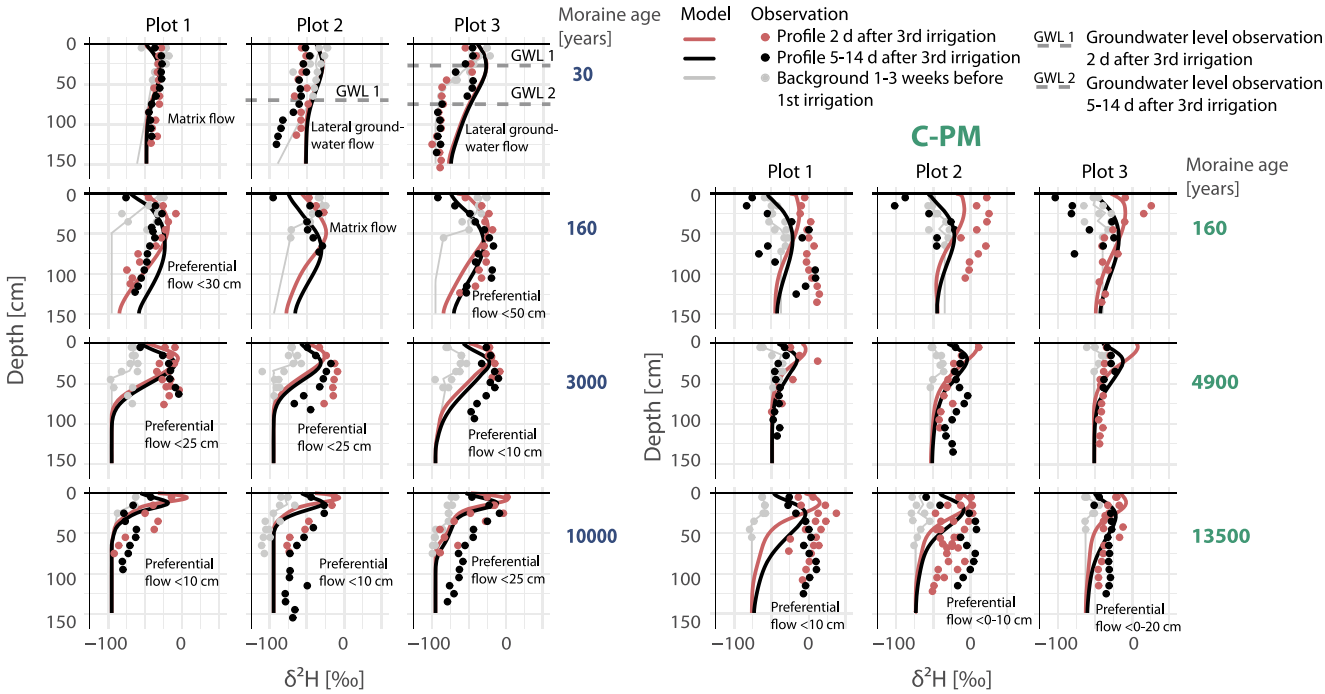

Figure 8. Measured and modeled δ^2H-isotope profiles after the irrigation experiments at both chronosequences, with the model assuming pure matrix flow.

lake and slope position of the two plots emphasizes the role of subsurface lateral water flow at the 30a moraine. At the 160a moraine (S-PM), the model overestimates deuterium concentrations below 60 cm in Plot 1 and underestimates them in Plot 3. Similar underestimations occur at the 3ka and 10ka moraines, indicating potential preferential water transport (Müller et al., 2014), as under preferential water flow conditions, the isotopic signal can reach greater depths faster than under matrix flow conditions (see also Section 3.2.3 where preferential flow occurrence is confirmed).

In Plot 1 and 2 of the 160a moraine at C-PM, the model underestimates the isotopic composition 2 days after the third irrigation. Plot 3 exhibits differences only in the upper 70 cm, with deviations below that being minimal. This underestimation suggests preferential water transport. The deuterium concentration of the second profile is mainly overestimated across all plots. However, this second δ^2H-profile, obtained the morning after a nocturnal snowfall event with an unknown δ^2H-concentration, significantly increases model result uncertainty. For the three plots of the 13.5ka moraine and Plot 2 at the 4.9ka moraine, the model underestimates the δ^2H-concentration, indicating potential preferential flow. In Plot 1 and 3 of the 4.9ka moraine, profiles show minimal depth variation, potentially resulting from simulated matrix flow. However, this low variability could also stem from high dispersivity and/or rapid vertical water transport, causing the isotopic signal to rapidly disappear.

3.2.2. Soil Moisture Signatures

The soil moisture signatures for each age class, parent material, and observation depth are displayed in Figures 9 and 10.

The five soil moisture signatures (Figure 4 and Table 3) describe the soil water dynamics in terms of velocity, relative timing of the peak, and magnitude. The irrigation signal reaches the sensors at C-PM faster than at S-PM (Figure 9). The response time (RT) increases slightly with age at both geologies. The time until the soil moisture peak is reached in relation to the end of irrigation (peak timing = PT, Figure 10a) reveals that especially the C-PM moraines reach the maximum water content already during irrigation (PT < 0). At S-PM this is mainly the case in the top soil at the 30a, 160a, and 3ka moraine. At the oldest S-PM moraine (10ka), the peak soil moisture is mostly reached after the end of irrigation (PT > 0). At the C-PM moraine, the available peak storage (PS, differences between the laboratory-based measured saturation water content and the peak soil moisture content) for the cases PT < 0 is relatively high (>20 Vol-%), which indicates that during the irrigation process the soil is not fully saturated and an equilibrium between infiltration and deep drainage is established. In

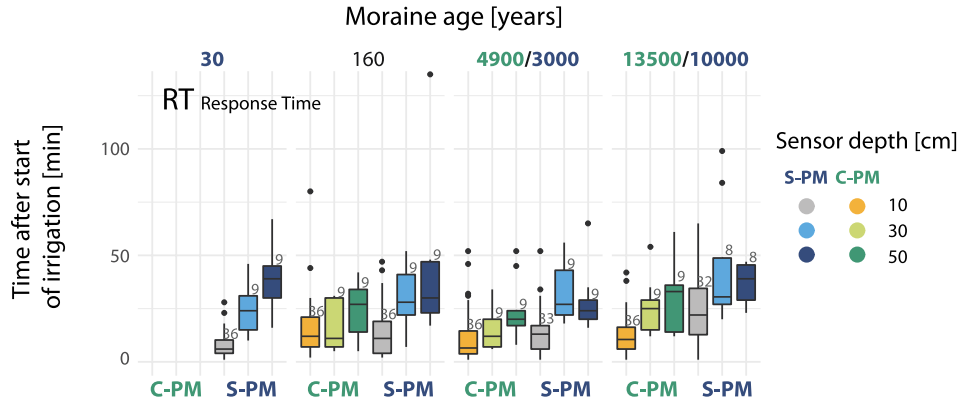

Figure 9. Soil moisture response time (RT) for age each class and sensor depth (10, 30, and 50 cm) for both geologies. Small numbers indicate the sample size of each box.

contrast, PS values at S-PM are small, which indicates that saturation occurs before the end of irrigation. High PS values indicating steady state flow were only found in 10 cm depth at the 3ka moraine. However, small differences and negative values should be interpreted with caution due to the uncertainties in the laboratory-based determination of the saturated water content and the uncertainties in the transferability of laboratory data to field measurements.

The relative maximum storage increase (SI) at the S-PM moraines is higher compared to C-PM. Especially in the topsoil of the 30a moraine and in 10 and 50 cm depth of the 10ka moraine at S-PM, SI mostly exceeds the irrigation input several times over (Figure 10c). A disproportionate increase in soil moisture could indicate lateral water input. At C-PM however, the relative maximum storage increase is consistently below the precipitation input. The relative event storage increase (ES), which describes the storage increase 3 hr after the event as fraction of the irrigation amount and provides information on water holding capacity, increases at S-PM from the young moraines to the old moraines, with the 3ka occasionally showing very high ES values. Compared to the maximum storage increase the event storage increase in the topsoil at the 30a and in 10 and 50 cm depth at the 10ka moraine is distinctly smaller. The event storage increase at C-PM is small with values consistently below 50% of the precipitation input.

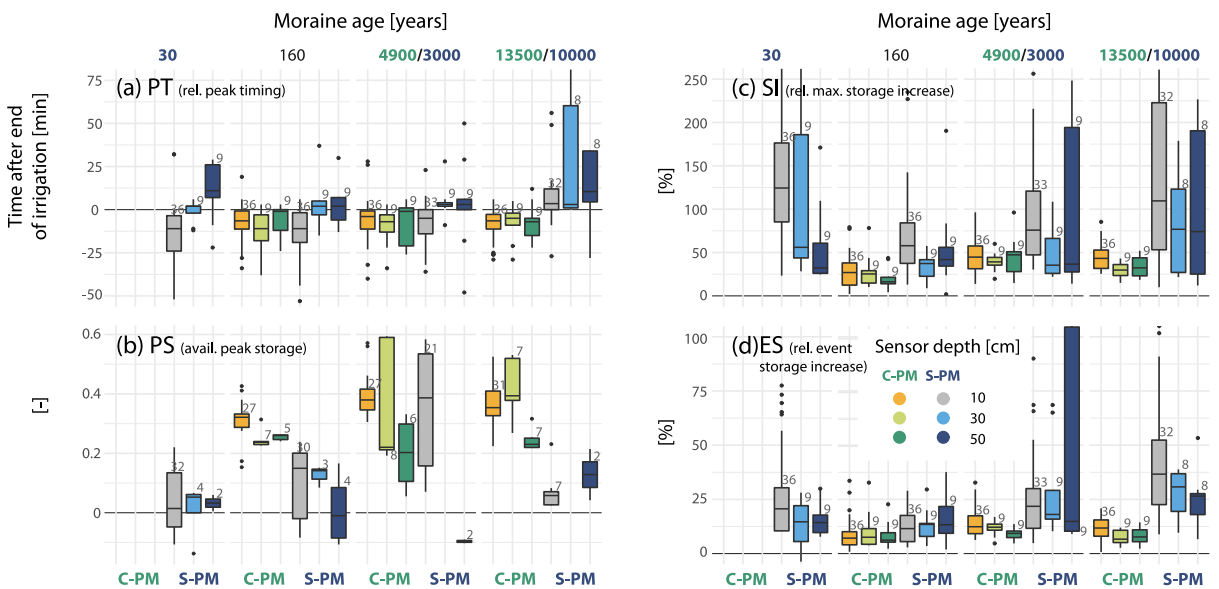

Figure 10. Timing of soil moisture peak relative to the end of irrigation (PT = relative peak timing) (a), difference between soil moisture peak and saturated water content (PS) for PT < 0 (b), relative maximum storage increase (SI) (c), and relative event storage increase (ES) (d) for all irrigation events at each geology, age class and sensor depth (10, 30, and 50 cm). Small numbers indicate the sample size of each box.

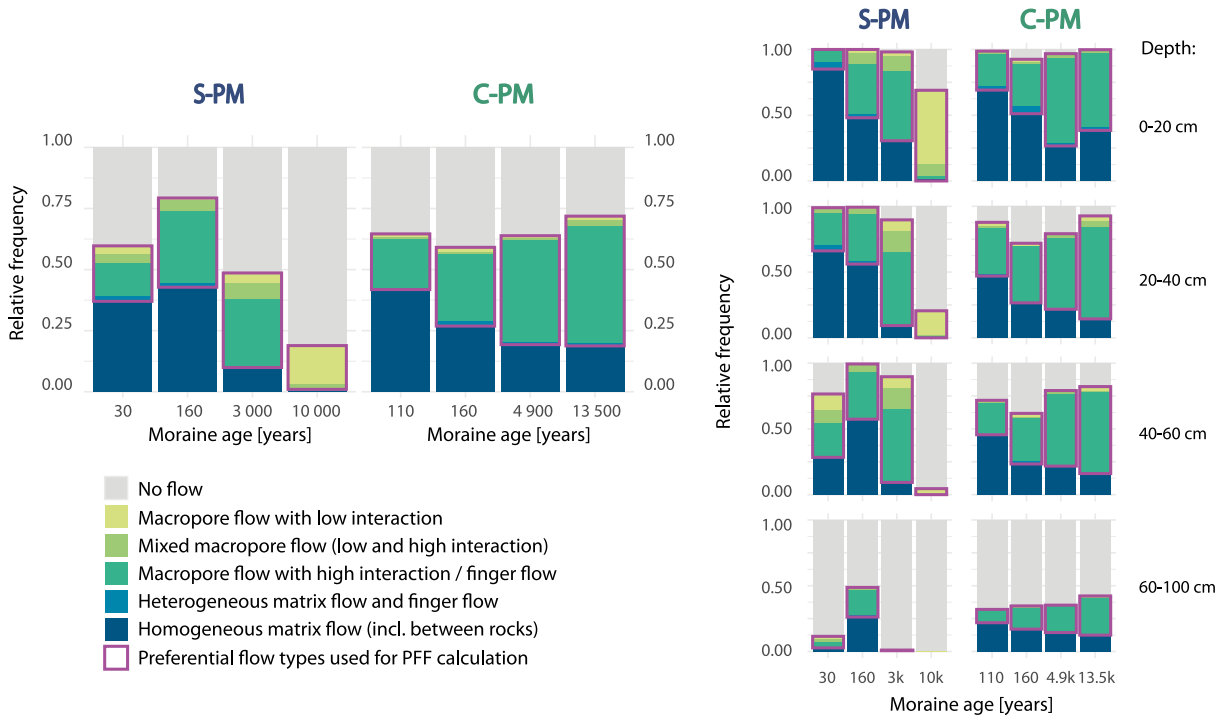

Figure 11. Evolution of flow type distribution at both chronosequences. Left: across the complete profile depth (Hartmann, Semenova, et al., 2020; Hartmann et al., 2022). Right: differentiated by depth. Magenta frames outline the preferential flow types used for the PFF calculation.

3.2.3. Dye Tracer Irrigation Experiments

Detailed results of the dye tracer experiments can be found in Hartmann, Weiler, and Blume (2020a) (S-PM) and Hartmann et al. (2022) (C-PM). Here we only give a brief summary of the observed flow types (Figure 11), which were then used to calculate the preferential flow fraction per profile. The flow pattern classification into flow types shows a decrease in matrix flow with increasing age at both geologies. At the calcareous site, matrix flow is more dominant, especially at the youngest age class, whereas at the oldest moraines finger-like flow is dominant. The two young moraines at the siliceous site are dominated by matrix flow. In the upper 20 cm the flow type frequency follows a clear age trend with an increase in preferential flow (finger-like flow and macropore flow) with increasing moraine age. At the 10ka moraine, the infiltration depth is distinctly lower compared to the younger age classes. This is the only moraine where macropore flow was observed, which is the dominating flow type at this age class. A significantly lower infiltration was also found below a depth of 60 cm at the 3ka and 30a moraine. The 30a moraine shows a high frequency of preferential flow at these depths. Preferential flow occurs here as funneling caused by large blocks of rock surrounded by clay and in form of macropore flow in cracks and finger like flow along material interfaces of a loam/clay horizon at 50 cm depth (Hartmann, Weiler, & Blume, 2020a).

We calculated the preferential flow fraction (PFF) as the occurrence of preferential flow observations (outlined in magenta in Figure 11) as fraction of all flow type observations (excluding no flow). PFF is displayed per geology, age class, and depth in Figure 12. No continuous age trend is observed for PFF in the top soil layer at the calcareous site, as the 4.9ka moraine shows the highest PFF. Only from a depth of 20 cm downwards do we observe a continuous increase in PFF with moraine age.

At the siliceous site, the fraction of preferential flow increases continuously with age in almost all three observation depths. An exception is the youngest moraine, where the proportion of preferential flow in 50 cm depth is higher than at the 160a moraine (median > 0.8). The highest PFF of all age classes at both parent materials was found at the 10ka moraine (siliceous parent material). Here we observed either no flow or a few preferential flow paths (macropore flow). The observation of preferential flow as the only flow type leads to PFF = 1.

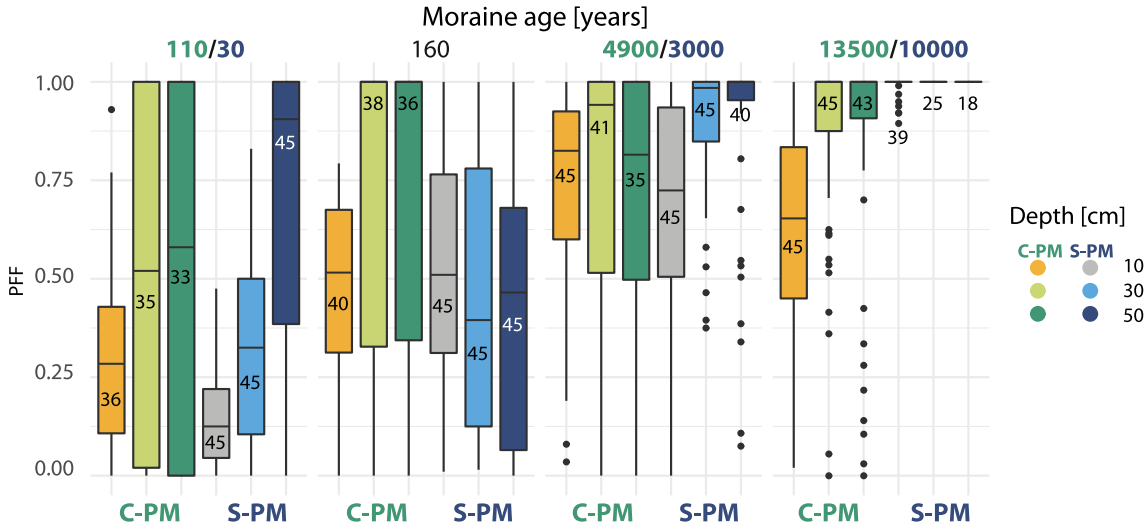

Figure 12. Preferential flow frequency as preferential flow fraction (PFF) at each age class of both geologies at 10, 30, and 50 cm depth. Numbers inside the boxes indicate the sample size. PFF = 1 means that only preferential flow was observed. At the 10ka moraine at S-PM mostly no flow or preferential flow was observed, resulting in PFF = 1 with almost no variability. Small numbers indicate the sample size of each box.

3.3. Links Between Hillslope Form and Hillslope Function

To investigate if clusters based on form (soil properties at 10 cm depth and vegetation/surface characteristics) show different behavior/functioning, we plotted the observed hillslope responses for each cluster in Figure 13. This figure also provides a summary of the cluster characteristics. The distribution of soil properties at 10 cm depth and vegetation/surface characteristics within each individual cluster is shown in Figure D1 in the Appendix D.

In Cluster 1, soil moisture signatures indicate steady-state transport conditions, soil saturation, and subsurface lateral flow. The peak soil moisture at 10 cm depth is mostly reached before the end of irrigation (PT < 0, Figure 13a-2). The available storage at peak soil moisture (PS) helps to identify, in cases of PT < 0, whether the peak soil moisture was reached due to saturation or an equilibrium between infiltration and deep drainage (described in detail in Section 2.5). At 10 cm depth, the PS values vary from 0 to 0.35 (Figure 13a-3), indicating that in some cases, saturation (PS close to 0) and in others, steady-state transport conditions (PS > 0) were reached. A relative maximum storage increase (SI) of more than 100% of the irrigation input indicates an additional water input through lateral flow (Figure 13a-4). At 10 cm depth, the median SI is around 50%, but the interquartile range reaches from about 30% to 120%, with a few outliers over 200%, hinting lateral subsurface flow. Surface and lateral subsurface flow (Figure 13b) were also directly observed (Maier & van Meerveld, 2021b; Maier et al., 2021). Cluster 1 has very high variations in preferential flow frequency (PFF) at 10, 30, and 50 cm depth. The median values increase with depth, but are always the smallest compared to the other clusters.

Cluster 2, in contrast, displayed exclusively steady-state transport conditions, with minimal lateral subsurface flow. The response times were slightly smaller compared to Cluster 1. In more than 80% of the observed sensor responses at 10 and 30 cm depth and more than 70% at 50 cm depth, the peak soil moisture was reached before the end of irrigation (PT < 0). The available storage at peak soil moisture (PS) in these cases exceeds 0.2 at all three depths, indicating solely steady state water transport conditions. Cluster 2 shows the smallest variation range in the relative maximum storage increase and the relative event storage increase. The preferential flow frequency increases with depth, reaching 1.0 at 30 and 50 cm depths.

Cluster 3 showcased cases of steady-state water transport and subsurface lateral flow, with longer response times across all depths compared to Clusters 1 and 2 (Figure 13a-1/7/13). At 10 cm depth, more than 60% of the soil moisture observations indicated a peak before the end of irrigation. In most cases of PT < 0 at 10 cm depth, the available peak storage is higher than 0.1, indicating that saturation was not reached and steady-state water transport was dominant. At 10 and 50 cm depths, in more than 25% of the observations, the maximum storage increase was higher than the irrigation input, indicating additional water input from lateral flow. Subsurface

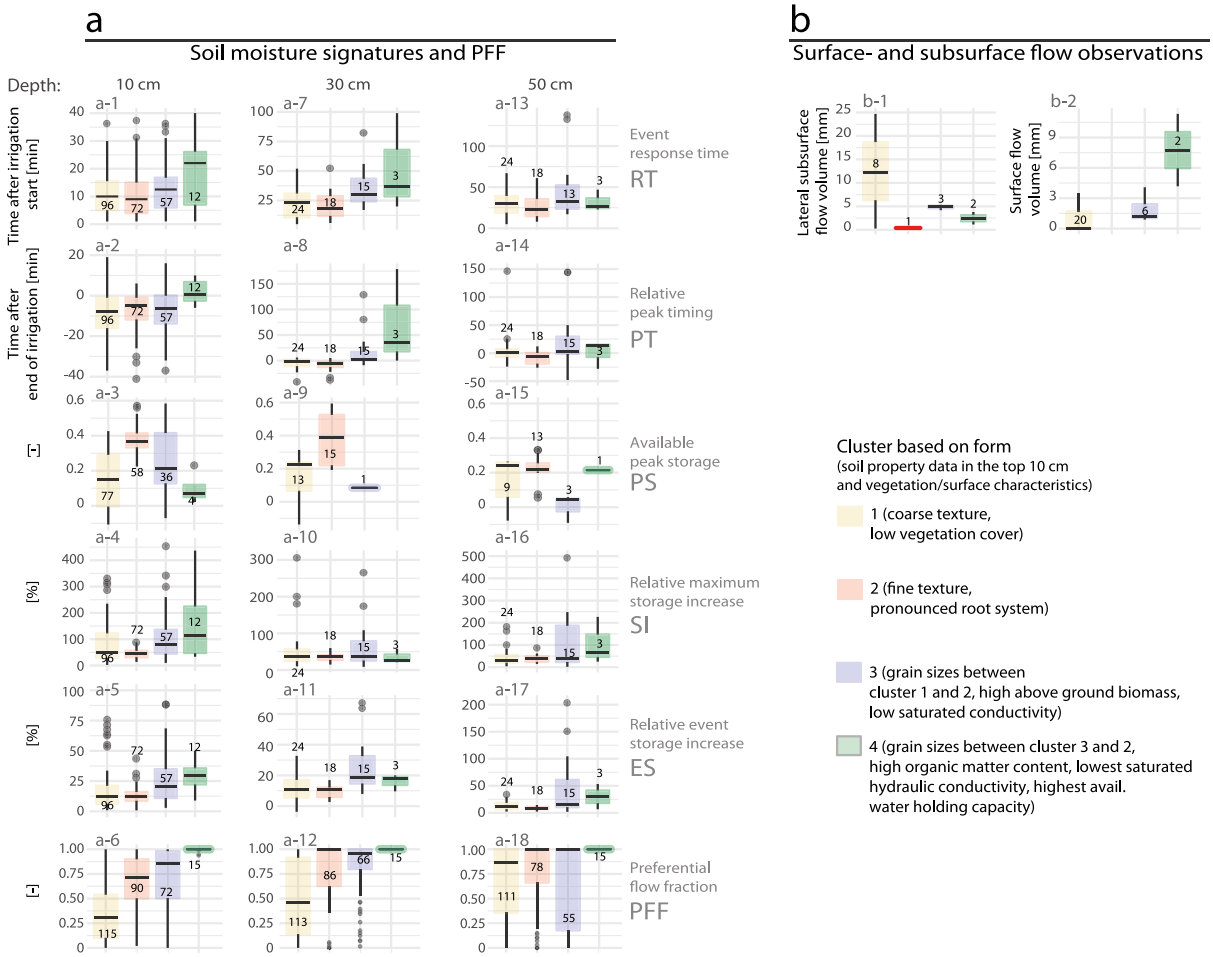

Figure 13. Left: Distribution of the soil moisture signature parameters and PFF in the four clusters based on form. Right: Surface- and subsurface flow observations by Maier et al. (2021) and Maier and van Meerveld (2021b) in the four clusters. Small numbers indicate the sample size of each box.

flow and surface flow were also directly observed by Maier et al. (2021) and Maier and van Meerveld (2021b) (Figure 13b). The preferential flow frequency was higher at 10 cm depth compared to Clusters 1 and 2.

Cluster 4, comprising only one experimental plot, exhibited high water storage capacities and subsurface lateral flow. The response time in cluster 4 at 10 cm depth is the highest of all four clusters. Only 25% of the observations at 10 cm depth showed a soil moisture peak before the end of irrigation. The maximum PT values are also distinctly higher in cluster 4 at 10 and 30 cm depths compared to the other clusters. The very few cases of PT < 0 showed an available peak storage between 0.05 and 0.2. The maximum storage increase at 10 cm depth is the highest compared to the other four clusters, and it is also the only cluster with a median maximum storage increase higher than the irrigation input, hinting at high lateral water transport. The preferential flow fraction is 1.0 at all three depths.

4. Discussion

4.1. Evolution of Hillslope Form

4.1.1. Grain Size Distribution and Structural Properties

The cluster analysis placed the young moraines of both geologies into a single cluster and the two older age classes into one cluster per geology (Figure 7) which suggests that age and geology determine differences in hillslope form, with age becoming less important and geology becoming more important as time progresses. The PCA reveals that differences in soil structural characteristics such as sand content and porosity as well as in

surface and vegetation characteristics such as microtopography, above ground biomass and root characteristics separate the old moraines of both geologies into different clusters. We find that at both geologies physical, chemical, and biological weathering processes cause a decrease in the sand content in favor of the silt and clay content (Figure 5). We assume that biological weathering processes (breakdown of particles by roots and root exudates) are constantly gaining in importance due to the advancing vegetation succession over the millennia of landscape development. The continuous biomass accumulation and the reduction in grain sizes with increasing age lead to an increase in porosity and a decrease in bulk density and thus to an increase in available water capacity.

However, there are some specific differences in the soil and landscape development between the parent materials that need to be discussed. We found finer grain sizes at the calcareous moraines (Figures 5a–5c), compared to the oldest siliceous ones, despite higher chemical weathering rates at the latter (Musso et al., 2022b). Apart from weathering processes, aeolian dust input can also be a cause for changes in the grain size distribution with increasing moraine age. Next to local aeolian depositions, the Alps consistently receive a minor dust input from the Sahara each year, with research suggesting non-constant deposition patterns over the past 10k years (Boxleitner et al., 2017; McGee et al., 2013). Consequently, the overall increase in fine particle content with the age of the moraines cannot be exclusively attributed to weathering. However, due to the proximity of our two study sites, we assume that the annual dust input is similar, in both geological settings, even with the awareness that deposition amounts can be influenced by slope exposition. Given the pronounced differences in grain sizes distribution between the parent materials, we assume that weathering processes are the dominant control here.

At the chronosequence of calcareous moraines, we did not observe a clear trend with age for some soil properties. Here, the clay content, organic matter content, and the porosity are higher at the 4.9ka compared to the 13.5ka moraine (plus correspondingly lower bulk density, Figure 5). This somewhat erratic development does not fit the evolution of soil properties observed in undisturbed systems (i.e., Douglass & Bockheim, 2006; Dümig et al., 2011; Vilmundardóttir et al., 2014). Also weathering indices derived by Musso et al. (2022b) indicated stronger weathering at the 4.9ka moraine compared to the oldest moraine of the same geology. We have to consider that in this case the assumption of the chronosequence approach that all moraines developed under the same environmental conditions and disturbances and only differ by their age is not completely valid. Different initial site conditions or/and geomorphological disturbances (Wojcik et al., 2021) may have led to different rates of change at these calcareous moraines, which led to a slightly higher development stage at 4.9ka. Evidence suggests that the 13ka moraine may has been exposed during the Dryas advance phases (Musso et al., 2020), which were colder and drier, potentially hampering soil formation. The Dryas advance phases denote cooling periods during the transition from the Last Glacial Maximum to the early Holocene, causing ice sheets and glaciers to advance (Ivy-Ochs et al., 2008). Consequently, the 13.5ka moraine would have experienced colder and drier climatic conditions in the initial years after exposure compared to the 4.9ka moraine, which was exposed during the Holocene. These climatic conditions may have slowed down the co-evolution of soil, water transport, and vegetation during the early stages at the 13.5ka moraine.

Moreover, it is essential to consider the diverse orientations of the plots on the moraines to explore whether they could account for the observed variations. North-facing slopes, receiving less direct sunlight, tend to have cooler temperatures and slower snowmelt, potentially influencing soil and vegetation development (Zapata-Rios et al., 2016). The three plots of the oldest moraine (13.5ka) all face north, while the plots on the 4.9ka moraine vary in orientation (north, south, and west) and might therefore have developed differently. However, Figure 7, displaying PCA results and clustering, indicates only subtle differences in soil, surface, and vegetation characteristics. All plots on both moraines are grouped in a single cluster and the range on the axes of the principle components is actually larger for the oldest moraine with respect to PC1 and similar to the 4.9ka with respect to PC2. Consequently, we infer that the differences in plot orientation on the 4.9ka moraine did not lead to significant differences in the evolution of hillslope form.

4.1.2. Available Water Capacity and Organic Matter Content

At the siliceous moraine chronosequence, organic matter development (derived here by loss on ignition) and available water capacity exhibit a continuous trend with a distinct increase between the two oldest moraines (Figures 5g and 5h). This is likely connected to vegetation cover, as the 3ka moraine is mainly dominated by grass, whereas the 10ka moraine has a dense vegetation cover consisting mainly of *Rhododendron ferrugineum* and *Vaccinium myrtillus*, both acid-loving species of ericaceous shrubs. The organic layer at the 10ka moraine has a high proportion of humus due to difficult to decompose substances such as lignin, cellulose and phenolic

compounds in the litter produced by the ericaceous shrubs (D'Amico et al., 2014; Pornon & Doche, 1996), positively affecting the available water capacity (Khaleel et al., 1981).

Despite the calcareous parent material having finer grained material (higher silt and clay content, Figure 5), the available water capacity on the siliceous moraines surpasses that of the calcareous moraines at older ages. The soil water retention curves, derived from laboratory analyses (Figure 7 in Hartmann, Weiler, & Blume, 2020a), reveal a clay-like to loamy-silty progression at the old siliceous moraine and a silty curve progression at the calcareous moraine. The high retention at the 10ka siliceous moraine is attributed to a substantial proportion of dead organic material, impacting structural variables (bulk density and porosity) and increasing soil absorption capacity (F. Yang et al., 2014). Despite the 3ka moraine having coarser texture and lower organic matter than the 4.9ka moraine, its available water capacity is higher. This discrepancy may be explained by the organic matter content, where living organic matter in form of a dense root network dominates at 4.9ka (Greinwald, Dieckmann, et al., 2021) and humus at 3ka, with the latter exerting a stronger influence on water retention (Greinwald, Dieckmann, et al., 2021).

4.1.3. Soil Formation and Vegetation Characteristics

The soil formation and vegetation characteristics at the old moraines exhibit distinct differences between the parent materials. Despite the existing literature on these study sites, the complex feedback mechanisms between vegetation development and soil formation in both forefields have not been thoroughly addressed, previously. Musso et al. (2022b) concluded that, concerning soil formation at the sites, the parent material plays a pivotal role until the later stages, where vegetation becomes more dominant. However, an explanation for the divergent development of vegetation cover between the two sites, resulting in varying effects on soil formation, was lacking.

We hypothesize that the interplay between parent material properties and vegetation coverage led to the faster vegetation colonization and distinct soil formation at the siliceous site. While the 160-year-old calcareous moraine was sparsely covered, its siliceous counterpart was fully vegetated, including ericaceous shrubs. In contrast, the 10,000-year-old siliceous moraine was already densely covered with these acid-loving ericaceous shrubs. We assume a positive feedback loop between pH levels and ericaceous shrubs, leading to a significant increase in shrub vegetation at the siliceous site. The low pH-values of the topsoil due to weathering of the siliceous parent material favor the settlement of ericaceous shrubs, which further lower the pH-value through litter production (Schaetzl, 2002) and root activities and which furthermore improves their own living conditions. Musso et al. (2019) reported at the siliceous site a steady decrease in pH from about 6.5 at the youngest moraine to about 4 at the 10ka moraine.

The dense growth of ericaceous shrubs may result from the cessation of grazing. Under low-pressure grazing, *Rhododendron ferrugineum* thrives, benefiting from its toxicity, which deters livestock and enables rapid spread (D'Amico et al., 2014; Ellenberg, 1988; Treter et al., 2002). This species tends to dominate subalpine landscapes, achieving up to 90%–100% vegetation cover (Pornon & Doche, 1996), especially on degraded soils (Costantini & Dazzi, 2013). The recovery of previously grazed areas leads to increased vegetation cover as existing shrubs spread (Scherrer & Pickering, 2005). The proximity to a local farm suggests that the 10ka moraine was likely grazed by sheep and goats, supported by reported trails indicating past livestock farming (Musso et al., 2020).

The high organic matter production and the low pH-value of the highly conductive, sandy soil at the 10ka moraine favor podsolization. Unlike Musso et al. (2019), who described the soil at the 10ka moraine as an entic podzol, we found a podzol with a clearly developed eluvial (albic) horizon overlying an iluvial horizon (Figure C1 in the Appendix C). A lack of the albic horizon was also occasionally observed, which explains different classifications by Musso et al. (2019, 2020), and Maier et al. (2020). The formation of podzol is also favored by the humid and cool-temperate climate in this area (Egli et al., 2001; Heikkinen & Fogelberg, 1980) and can lead to the formation of hard pan, which was present here at an early stage as solidified soil.

The calcareous moraines displayed a delayed process of vegetation coverage, accompanied by similar short-term erosion rates and even lower long-term erosion rates compared to the siliceous moraines (Musso et al., 2022b). Despite these dynamics, the soil production in the early stages still lags behind soil denudation rates. At the calcareous site, the 13.5ka moraine showed a similar vegetation cover as the 4.9ka moraine. Both moraines are mainly covered with grass. The soil pH at the calcareous chronosequence does not change much over the millennia (mostly between 7 and 8) (Musso et al., 2019), since the carbonate-rich soil material buffers the organic and carbonic acids. We posit that the higher pH levels create an environment less conducive to the rapid settlement

10.1029/2023WR035937

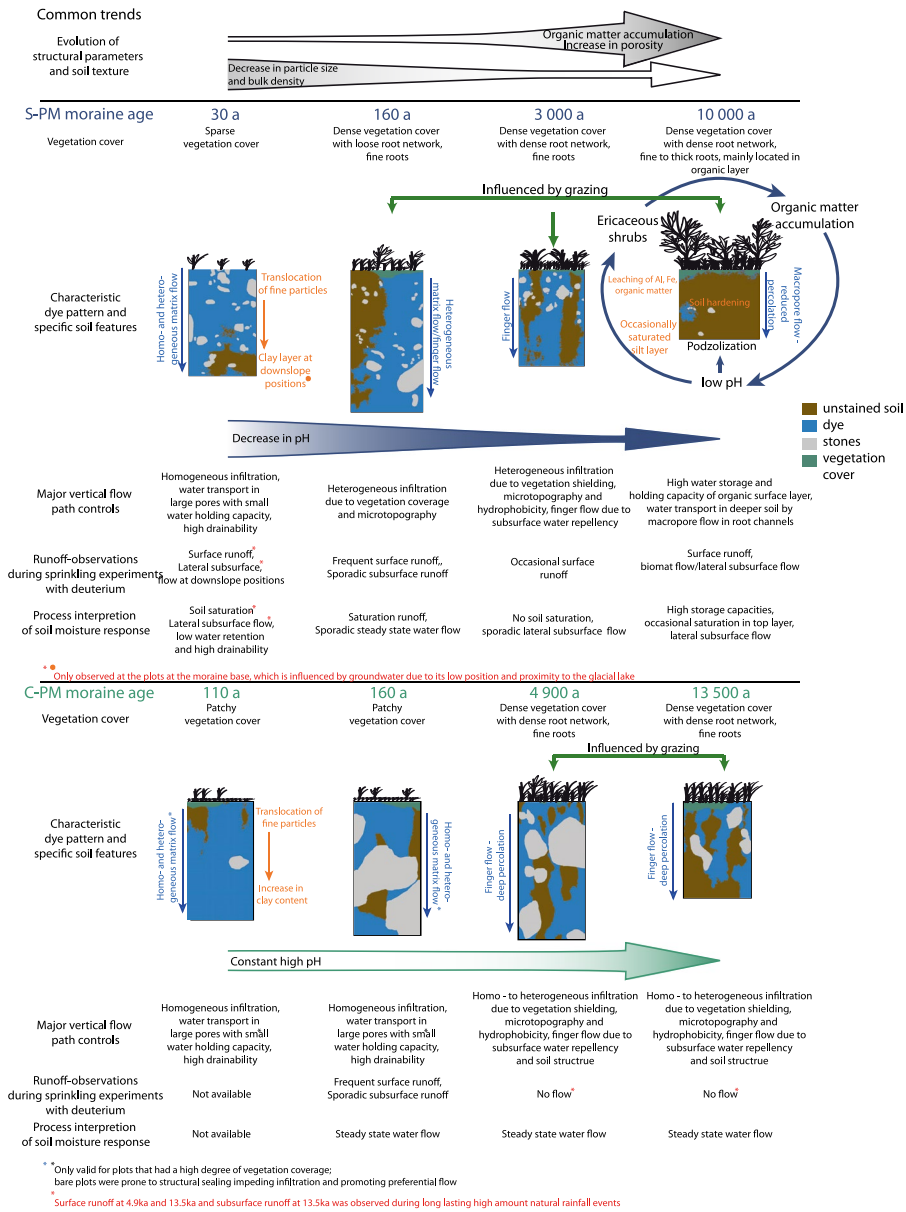

Figure 14. Sequence of observed vegetation characteristics, runoff observations, dye pattern characteristics and soil features (process and properties) along the chronosequences at S-PM and C-PM. Figure adapted from Hartmann, Semenova, et al. (2020).

of litter-producing vegetation, resulting in a diminished organic matter input compared to the siliceous site. Accordingly soil formation at the calcareous site was not as distinct. Compared to the soil at the young moraines, a color change to a more brownish hue can be seen in the upper 50 cm of the old moraines, but weathering and soil formation are less profound compared to the old moraines on siliceous parent material (Musso et al., 2022b). The soil material at greater depths still very much resembles the material of the young moraines.

4.2. Evolution of Hillslope Function and Links to Form

The relevant observations on soil development, vegetation cover and dominant flow components are summarized in Figure 14 and supplemented with information on the occurrence of surface and subsurface runoff during the irrigation experiments by Maier and van Meerveld (2021b) and Maier et al. (2021). At the siliceous site we found a distinct transition in water transport processes over the first millennia of landscape evolution (Figures 8–12).

The coarse textured young soil at the 30a moraine has a low water retention and high drainability. The water transport is dominated by fast vertical water movement. Only the plots located down-slope in close proximity to the glacial lake showed subsurface flow caused by near-surface groundwater and saturation excess overland flow during the irrigation experiments. At the intermediate age classes the soil water storage capacity increases due to the reduction in grain sizes and organic matter accumulation. The water transport is mainly vertical and increasingly preferential in form of finger-like flow (Figure 11) caused by surface structure and hydrophobicity (Hartmann, Semenova, et al., 2020). Saturation runoff and lateral flow was observed but rarely occurred. At the oldest moraine of 10k years, surface and lateral subsurface flow as well as water storage in the organic surface layer play the dominant role in water redistribution (Figure 10). Vertical water transport beyond the organic top layer by macropore flow along root fissures was observed, but contributes little to the water redistribution. Only a few flow paths that went beyond the organic layer were observed during the dye tracer experiments (Figure C1).

The results are similar to findings by Lohse and Dietrich (2005) who found a transition from mainly vertical to lateral water transport processes between a 300-year-old Andisol and a 4.1 million-year-old Oxisol. Also Yoshida and Troch (2016) reported a transition of the major flow pathways from deep percolation to more shallow subsurface flow with increasing age of volcanic catchments. In contrast to the findings by Lohse and Dietrich (2005), our study at the siliceous site found that the transition of major water flow paths from vertical to horizontal is not caused by the accumulation of clay particles. Lateral subsurface flow and biomat flow occurs due to the progressive accumulation of organic matter that initiates podzolization and the concomitant subsurface consolidation. Thus, at the 10ka, the organic layer plays an important role in water redistribution. The high eco-hydrological significance of the organic horizon in alpine regions was also pointed out by F. Yang et al. (2014). The high water retention capacity of the organic layer captures large amounts of rainfall and prevents further percolation. This explains why surface runoff and lateral subsurface flow occurred only on the second or third day of irrigation (Table A1) together with deep percolation via preferential flow (Figure 8). We assume that the first irrigation filled the storage of the organic layer to such an extent that the water input of the following days led to saturation runoff and to lateral subsurface runoff. As the hydraulic conductivity of organic soils is highly anisotropic with higher conductivities in the lateral than vertical direction (Beckwith et al., 2003; Chason & Siegel, 1986), lateral flow probably occurred in form of biomat flow within the organic layer and along the interface with the underlying less permeable soil material. The high water retention of the organic layer leads to a high water availability, which has a positive effect on the vegetation and thus in turn again on the organic matter content (Y. Yang et al., 2009). This creates a positive feedback loop between soil moisture and organic matter content, which was primary set in motion by the low pH value in the siliceous material and therefore delayed conversion of the raw humus.

In contrast to the siliceous parent material, water transport processes did not change significantly in the first millennia of landscape development at the calcareous site. The water transport at all moraines is dominated by fast vertical water movement (Figure 10). The water is transported mainly via matrix flow at the young moraines, which becomes more preferential (finger-like flow) with increasing moraine age (Figure 11). In most cases, an equilibrium between infiltration and drainage was observed without saturation of the topsoil. Only at the 160a moraine, surface runoff was observed during the irrigation experiments (the experiments were not conducted on the 110a moraine). Runoff at this moraine is probably caused by the dense stone cover but also structural sealing was observed, which partly led to a reduced infiltration capacity (Hartmann et al., 2022; Maier et al., 2021). The transport velocity decreased and the storage capacity increased from the young to the old moraines, which is caused by the decrease in particle sizes and increase in organic matter content. However, the development is not continuous with age. Storage properties are highest at the 4.9ka moraine followed by 13.5ka moraine and the lowest at the youngest moraine, which correlates with the organic matter content (Figure 6).

The distinct differences in the hydrologic response evolution in the two glacier forefields show that age alone cannot be used as a control variable to predict hydrological responses in ungauged landscapes. It is therefore advisable to consider the (hydrological) age of a catchment according to the concept of Troch et al. (2015), which defines hydrological age (here applied to hillslopes) as a function of the activity of the catchment-forming factors driving coevolution (climate, geology, and tectonics). In this concept, the disparity in the hydrological response between an observed system state and the initial system state is used as a measure for the (relative) hydrological age. The activity level of the drivers (climate, geology, and tectonics) reflects the potential for processes associated with these drivers to influence the hydrological response. The higher the impact of these processes on a

change in the hydrological response, the greater the activity level associated with this driver, implying a proportional relationship between the activity and the rate of change in the hydrologic response.

Under nearly the same climate and tectonic history, the activity of the siliceous geology, driving the co-evolution of vegetation, soil, and hydrologic response, seems to be higher compared to the calcareous parent material. The hydrological response at the siliceous site exhibits a significant divergence between the youngest and oldest moraines, whereas at the calcareous site, the disparities in the hydrological response between the young and old moraines are less distinct. Drawing from Troch et al. (2015), an index for chemical weathering was suggested to describe geology activity. Consistent with this, chemical weathering rates at the siliceous site were found to be higher than at the calcareous site (Musso et al., 2022b), aligning with the insights of Troch et al. (2015).

However, the activity level of geology is not completely independent of the other driving factors. The occurrence of podsolization in the siliceous material as a result of weathering and translocation processes is largely attributed to the cool and humid climate, which favors the accumulation of organic matter and the translocation of organic acids. Comparing both geologies in different climatic settings may lead to different results and activity levels of the parent material.

4.3. General Links Between Hillslope Form and Hillslope Function

The identification of links between the hydrological response and structural features independent of developmental stage would allow for a first assessment of the hydrological response in ungauged landscapes using easily measured/observed variables. This would contribute significantly to the fundamental processes of knowledge transfer and the identification of process similarities of hydrological systems (Blöschl, 2016). We derived general links by testing whether different clusters of hillslopes identified by variables describing form are also different in their hydrological response. The form-and-function dualism in hydrology, explored in Angermann et al. (2017), Fan et al. (2020), and Gnann et al. (2021), emphasizes the importance of observation scale and selecting appropriate variables for assessing form-function relationships in heterogeneous environments. Our data set employs commonly used variables in environmental science studies (e.g., ecology, botany, geomorphology, geography).

To this end we carried out a cluster analysis of soil structure and vegetation/surface characteristics at each plot, independent of age and parent material. We found that the presence of a thick organic layer is linked to high storage properties. The comparatively high storage properties in cluster 4 (Figure 13), which were identified by the longest response times, positive peak timings and largest storage increase, are linked to a high amount of organic matter content of various decomposition stages, which goes along with a high available water capacity. The presence of an organic top layer was also found to be a good indicator for the occurrence of lateral subsurface flow in clusters 3 and 4. Lateral flow was indicated by the occurrence of relative maximum storage increase values of >100% and was furthermore observed at the trenches of the irrigation plots (Maier et al., 2021). Similar findings in alpine grassland were reported by F. Yang et al. (2014) who also found high storage capacities in the organic layer, together with lateral subsurface flow. The lateral subsurface flow observed in cluster 1 is, however, likely driven by the hillslope position at the footslope.

The soil textural information alone is not found to be a good predictor of hillslope hydrological response. We found that its impact can be obscured by the organic matter content. The grain size distribution in cluster 4 is in a similar range as in cluster 1 (Figure D1 in the Appendix D). However, due to the high organic matter content in cluster 4, porosity and bulk density, and the hydrological response are significantly different from cluster 1. The positive effect of organic matter on soil water retention is widely known (Rawls et al., 2003), and information on organic matter content is already an essential feature within the hydrological characterization of soils (e.g., via pedotransfer functions Pachepsky & Van Genuchten, 2011). Nevertheless, our findings also emphasize the crucial role of the type of organic matter in predicting its hydrological impact. Our assessment of organic matter did not distinguish between living (e.g., roots) and dead (detritus or humus) organic matter. However, based on observations in the field, we can say that in comparing cluster 2 and 3, the main part of the organic matter in cluster 3 is made up of dead organic material, while cluster 2 has a high content of active root material. By comparing cluster 2 and 3 in regard to their observed properties, we found that despite having a lower organic matter content and a coarser grain size distribution (also lower porosity and higher bulk density), the vertical saturated hydraulic conductivity in cluster 3 is also lower. Interestingly, the hydrologic response in cluster 3 shows more water storage and occasional lateral subsurface flow, whereas cluster 2 shows little water storage and mainly steady-state

vertical water transport. A high proportion of dead organic material (as in cluster 3) is known to have a decreasing effect on saturated hydraulic conductivity (Demir & Doğan Demir, 2019; Jarvis et al., 2013), whereas the dense root network of grassland vegetation (as in cluster 2) enhances infiltration by providing additional flow paths for water transport (Leimer et al., 2021).

We found that the occurrence of preferential flow is closely linked to vegetation characteristics as above ground biomass (Figure 13) and the architecture of the root system (Figure D1). The strength of this relationship might in part be due to the chronosequence study design where we cannot evaluate the impact of biomass/root systems and soil characteristics independent of each other. We observed a transition from homogeneous unconsolidated coarse textured soil (cluster 1) to a layered soil system (cluster 2 to 4), which together with vegetation development leads to the formation of finger-like flow paths (cluster 2–3) and macropore flow (cluster 4). The above ground biomass, which decreases from cluster 1 to 4 is an indicator for the change in vegetation. The vegetation develops in clusters 1 to 3 from small pioneer plants to grassland (clusters 1 and 2) to herbaceous to shrub vegetation (cluster 3). Cluster 4 is dominated mostly by shrub vegetation. This development also influences the infiltration pattern, which becomes increasingly heterogeneous from cluster 1 to 4. With the type of vegetation cover, the root system also changes, which also has a major impact on PFF. The specific root length increases from cluster 1 to 4. High SRL values indicate root systems made up of long and thin roots, while smaller values indicate shorter, thicker roots. The pattern across the clusters matches the vegetation observation. The small pioneer plants in cluster 1 have very fine and long roots, which theoretically could form preferential flow paths (Ghestem et al., 2011), but their effect on water transport is small compared to abiotic factors (coarse textured soil). For the grass vegetation in clusters 2 and 3, the root network is already denser and the roots larger, which (among other factors) promotes the formation of finger-like flow paths. The shrub vegetation in cluster 4 primarily develops near-surface, woody roots. The high proportion of preferential flow is due to the small amount of water that preferentially infiltrates macropores beyond the organic layer. We conclude that in our chronosequence study the occurrence of preferential flow is closely linked to vegetation characteristics as above ground biomass and the architecture of the root system. This also confirms the findings described in Hartmann, Semenova, et al. (2020) and Hartmann et al. (2022).

While saturated hydraulic conductivity is often used as an indicator in the context of land use/cover changes and the impact on hydrological flow paths such as overland flow and subsurface stormflow (Archer et al., 2013; Godsey & Elsenbeer, 2002; Tian et al., 2017; Zimmermann et al., 2006), it did not work well as an indicator for either preferential nor lateral surface/subsurface flow in our study. We observed an increase in PFF with decreasing saturated hydraulic conductivity, but the magnitude of hydraulic conductivity is more of an indicator for the progression of weathering and soil formation processes that also lead to change in the vertical subsurface flow paths.

5. Conclusions

Our investigation of the evolution of hillslope form and function in two glacier forefields with different parent material shows that chemical composition of the parent material affects the hydrological functioning. Soil pH seems to be the key variable that determines vegetation development, soil formation (hillslope form) and subsequently hydrology (hillslope function). The sites in our study are exposed to approximately the same weathering conditions. Although the calcareous material breaks down faster into finer-grained material, it is the acidic weathering of the siliceous material that has a profound impact on water storage and transport. The acidity resulting from the weathering of siliceous material creates an environment conducive to the growth of shrub vegetation, leading to higher organic matter production. Simultaneously, it facilitates the preservation of organic material. Combined with increased inputs from shrub vegetation, this results in a significant accumulation of dead organic matter. The organic matter accumulation then significantly alters storage and transport properties by increasing water storage capacity.

Water redistribution is dominated by vertical subsurface water transport only in the two youngest age classes. Podzolization occurs on the siliceous parent material sometime between 3,000 and 10,000 years of landscape development. After 10,000 years of soil development water storage in the organic surface layer, lateral subsurface water transport and overland flow become the major components controlling water redistribution. At the calcareous site, the high pH-buffering capacity of the soil leads to less soil formation and fast, vertical subsurface water transport dominates the water redistribution even after more than 10,000 years of landscape evolution.

It is unclear whether the differences in hydrologic flow paths in turn impact the vegetation development. We assume that at the siliceous site, the increase in storage in the topsoil triggered a positive feedback cycle and that the increase in water and nutrient availability favored the settlement of ericaceous shrubs, which in turn have a positive effect on the storage capacity of the soil. At the calcareous site, on the other hand, important plant nutrients are likely to be leached and thus lost from the root zone. This limits the development of larger vegetation which could improve the storage capacity in the topsoil by organic matter production.

Our study showed that form and function develop differently on chemically different parent materials, making the parent material an important proxy for linking form and function. The partitioning into surface and subsurface lateral flows, as well as the development of subsurface vertical flow paths, is clearly influenced by weathering and soil development. It is also, to a large extent, shaped by accompanying vegetation and soil formation, significantly impacting the local water budget. We found that the interplay between geology, vegetation, and the occurrence of an organic surface layer are essential landscape features that are linked with the hydrological response and should be considered when reading and interpreting the landscape to assess the hydrological functioning of ungauged areas.

The accelerated retreat of glaciers exposes more and more young alpine landscapes, which will undergo pronounced changes within a few decades and centuries. Our study contributes to predicting the future evolution of local hydrology in these emerging landscapes. The benefit of our findings is, however, not only limited to the application in proglacial areas, but could also be used in the context of renaturation of degraded hillslopes. Incorporating our findings in landscape evolution models could improve the proper description of the hydrological response within these models. We would furthermore stress that we were only able to make these findings by collaborating closely across disciplines. We see this kind of interdisciplinary approach including joint data collection and interpretation as indispensable to assess developments of hydrological systems, especially in the context of climate change.

Appendix A: Ratios of Surface and Subsurface Runoff During the Irrigation Experiments

Table A1 shows the ratios of surface and subsurface runoff during the irrigation experiments with deuterium. Each plot at each moraine was irrigated for 3 days with three different irrigation intensities and deuterium-concentrations. The data shows that subsurface water transport processes dominate the transport processes at both forefields.

Water Resources Research

10.1029/2023WR035937

Table A1

Ratio of Surface[a] and Subsurface Runoff[a] of the Irrigation Water for all Three Irrigation Plots and Intensity per Age Class at the Siliceous and Calcareous Forefield

	Irrigation		Irrigation		Irrigation	
	Day 1		Day 2		Day 3	
Plot 1	Surface runoff ratio (%)	Subsurface runoff ratio (%)	Surface runoff ratio (%)	Subsurface runoff ratio (%)	Surface runoff ratio (%)	Subsurface runoff ratio
Moraine						
Siliceous						
30*a*	0	0	0	0	4	0
160*a*	0	0	0	10	2	8
3*ka*	0	0	0	0	3	0
10*ka*	0	0	42	4	22	20
Calcareous						
160*a*	3	0	7	0	11	0
4.9*ka*	0	0	0	0	0	0
13.5*ka*	0	0	0	0	0	0

	Irrigation		Irrigation		Irrigation	
	Day 1		Day 2		Day 3	
Plot 2	Surface runoff ratio (%)	Subsurface runoff ratio (%)	Surface runoff ratio (%)	Subsurface runoff ratio (%)	Surface runoff ratio (%)	Subsurface runoff ratio
Moraine						
Siliceous						
30*a*	11	44	11	81	6	92
160*a*	16	0	6	0	5	0
3*ka*	0	0	17	0	9	0
10*ka*	0	0	0	10	11	19
Calcareous						
160*a*	0	0	10	0	5	3
4.9*ka*	0	0	0	0	0	0
13.5*ka*	0	0	0	0	0	0

Water Resources Research

10.1029/2023WR035937

Table A1
Continued

	Irrigation		Irrigation		Irrigation	
	Day 1		Day 2		Day 3	
Plot 3	Surface runoff ratio (%)	Subsurface runoff ratio (%)	Surface runoff ratio (%)	Subsurface runoff ratio (%)	Surface runoff ratio (%)	Subsurface runoff ratio
Moraine						
Siliceous						
30*a*	8	78	11	32	11	55
160*a*	0	0	4	0	3	0
3*ka*	0	0	0	0	0	14
10*ka*	0	0	6	0	5	0
Calcareous						
160*a*	6	0	4	0	5	1
4.9*ka*	0	0	0	0	0	1
13.5*ka*	0	0	0	0	0	0

[a]This data was compiled from and can be accessed via Maier and van Meerveld (2021a).

Appendix B: Calibration of the Longitudinal Dispersivity for One-Dimensional Water Transport Modeling

To model the water transport with HYDRUS-1D, the longitudinal dispersivity (D_L) was determined by manual calibration. For simplicity, D_L was assumed to be constant with depth. For the calibration, the model was executed with seven different values for D_L (0.1, 0.5, 1, 1.5, 3, 5, 10, and 15 cm). A visual comparison of the model output with the measured isotope profile (Figures B1and B2) was used to identify the best fit. The resulting longitudinal dispersivities are listed in Table B1. D_L decreases with increasing moraine age. Moraines at the siliceous site have lower dispersivities than at the calcareous site.

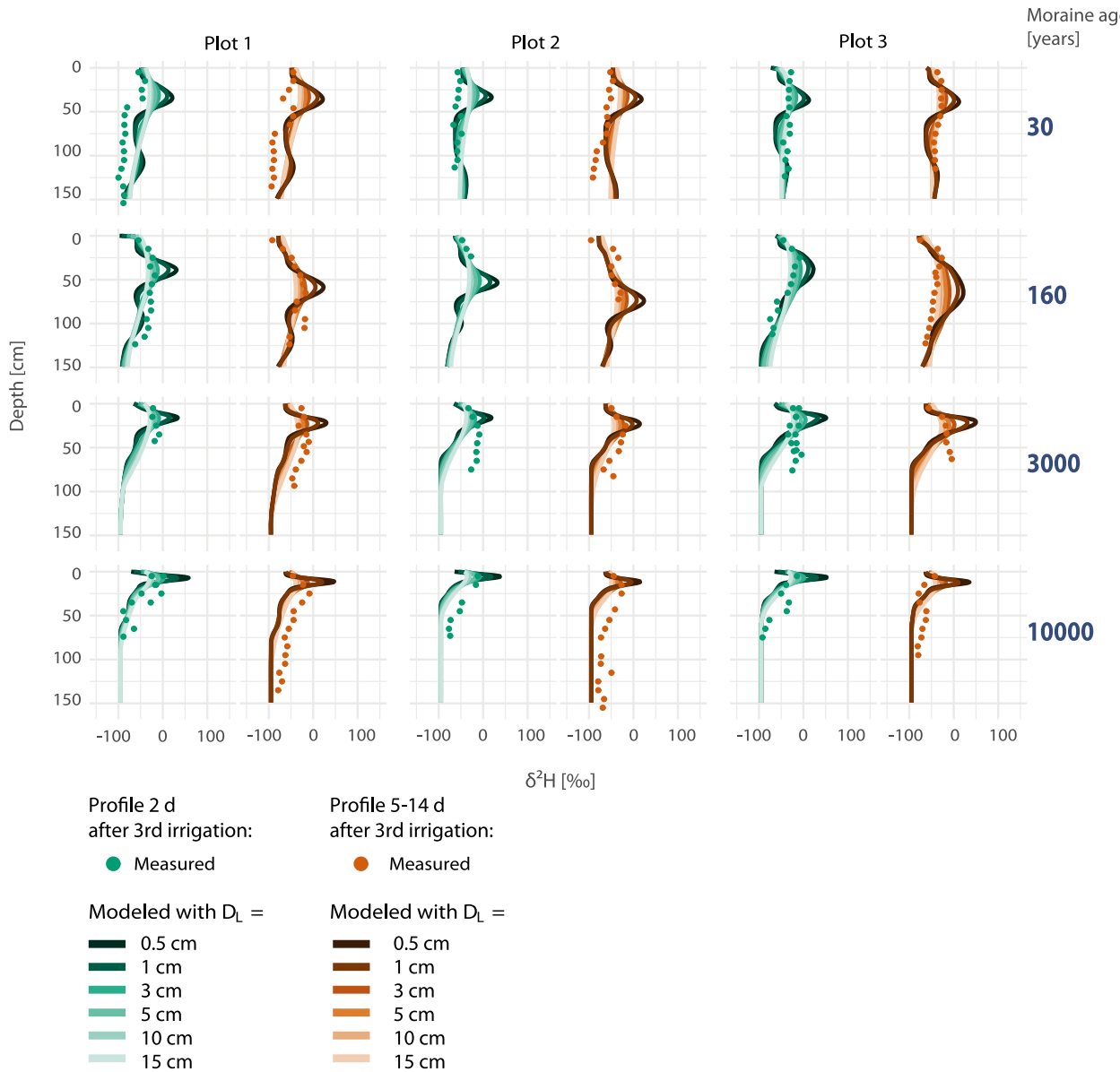

Figure B1. Manual calibration of the longitudinal dispersivity (D_L) for the siliceous parent material (S-PM). Displayed are modeling results of the δ^2H-profiles with seven different values for D_L (0.1, 0.5, 1, 1.5, 3, 5, 10, and 15 cm) compared to the field observations. A visual validation was used to estimate which order of magnitude of D_L is most realistic for the δ^2H-transport. Modeling results and observations of the profiles taken 2 days after the third irrigation are displayed in green shades. Orange shades show the modeling results and observations of the profiles taken 5–14 days after the third irrigation.

10.1029/2023WR035937

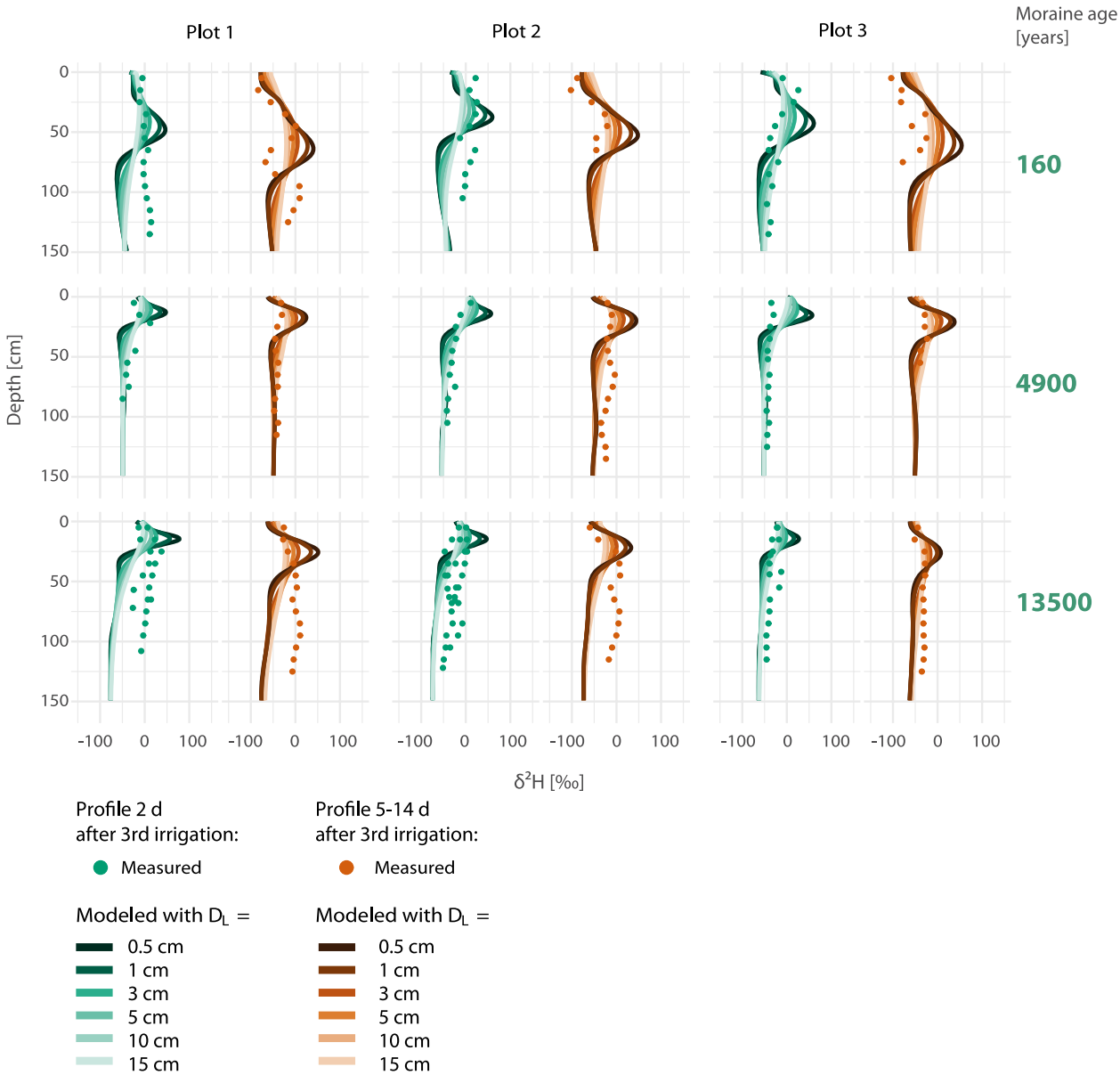

Figure B2. Manual calibration of the longitudinal dispersivity (D_L) for the calcareous parent material (C-PM). Displayed are modeling results of the δ^2H-profiles with seven different values for D_L (0.1, 0.5, 1, 1.5, 3, 5, 10, and 15 cm) compared to the field observations. A visual validation was used to estimate which order of magnitude of D_L is most realistic for the δ^2H-transport. Modeling results and observations of the profiles taken 2 days after the third irrigation are displayed in green shades. Orange shades show the modeling results and observations of the profiles taken 5–14 days after the third irrigation.

Table B1
Dispersion Coefficients at the Siliceous (S-PM) and Calcareous (C-PM) Parent Material Estimated by Visual Calibration

S-PM		C-PM	
Age	D_L (cm)	Age	D_L (cm)
30*a*	10		
160*a*	7	160*a*	15
3*ka*	5	4.9*ka*	10
10*ka*	3	13.5*ka*	5

Appendix C: Photographs of Typical Flow Patterns at Each Age Class

Figure C1 shows examples of the observed subsurface flow paths highlighted by blue dye at the four moraines at the siliceous (S-PM) and calcareous (C-PM) parent material. The soil classification according to the World Reference Base for Soil Resources (IUSS Working Group WRB, 2014) was done by Musso et al. (2019, 2020), and Maier et al. (2020) at the same moraines, but different soil pits. Unlike (Musso et al., 2019), who described the soil at the 10-year-old moraine as an entic podzol, we found a podzol with a clearly developed eluvial (albic) horizon overlying an iluvial horizon. The soil below the eluvial horizon was solidified and only a few single roots and flow paths were observed in this depth during the dye tracer experiments.

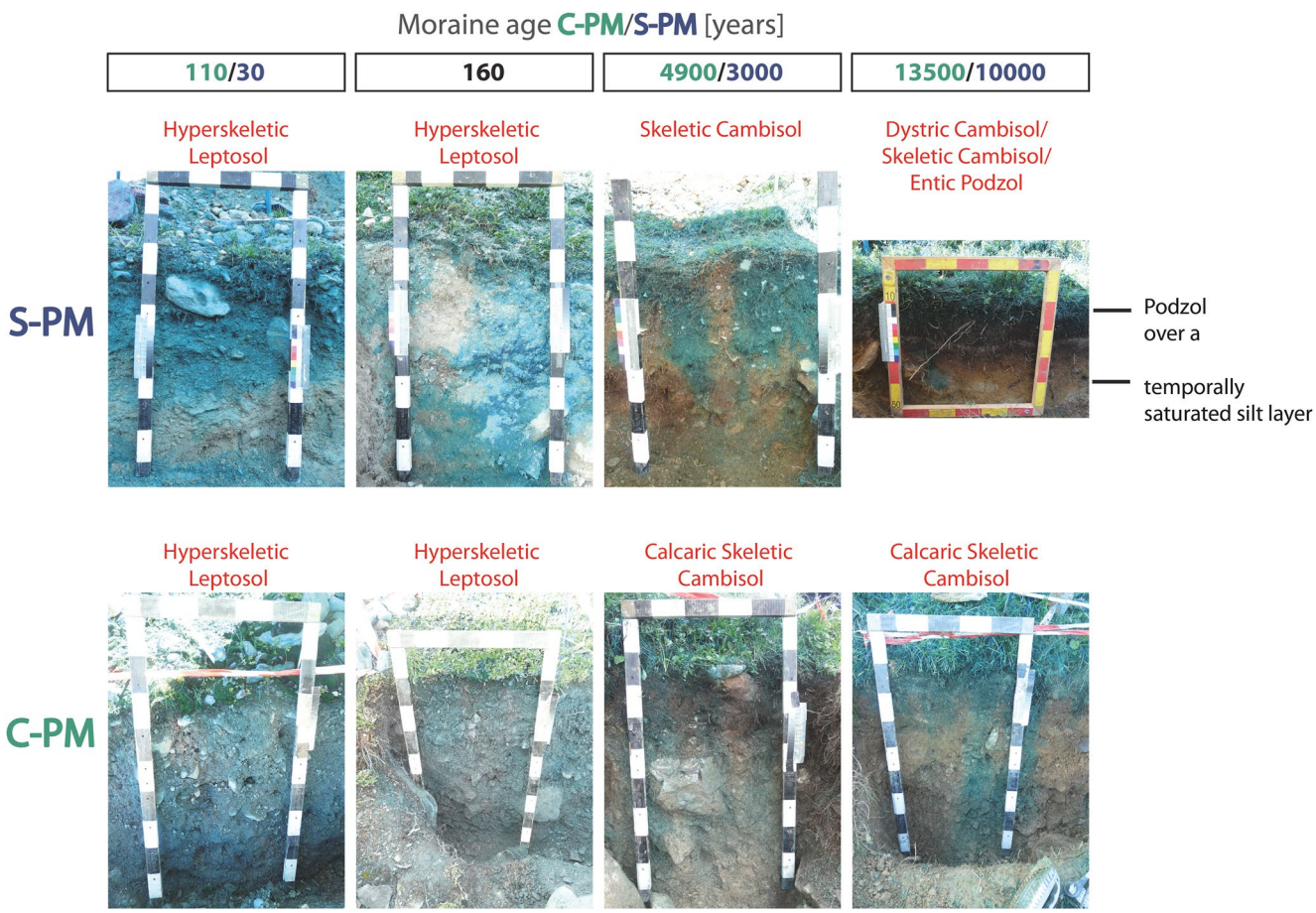

Figure C1. Examples of the observed subsurface flow paths highlighted by blue dye at the four moraines at S-PM and C-PM. In red: the WRB (IUSS Working Group WRB, 2014) soil classification (Maier et al., 2020; Musso et al., 2019, 2020). Black: Additional observations during the profile excavations. The length of each segment of the wooden frame equals 10 cm.

Appendix D: Distribution of Soil Properties and Surface Characteristics Within Each Cluster

The clusters in Section 3.1.2 were determined based on a prior principal component analysis of the set of form variables (soil surface properties, surface characteristics and vegetation characteristics). Figure D1 shows the distribution of each of these characteristics within each cluster. PFF (Figure 13), above ground biomass (BM), specific root length (SRL), and saturated hydraulic conductivity (Ksat, Figure D1) show a similar distribution pattern across the clusters (with SRL and Ksat showing an inverse distribution).

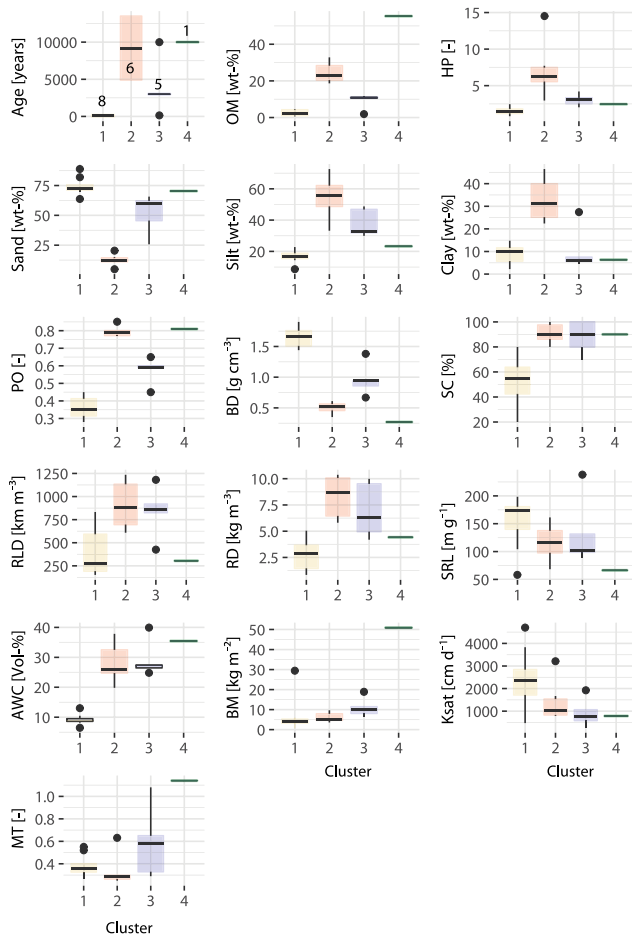

Figure D1. Boxplots showing the distribution of age, soil properties at 10 cm depth, and surface/vegetation characteristics within the four clusters. Clusters were derived based on a principal component analysis using the shown soil properties and surface/vegetation characteristics. An explanation of the abbreviations is given in Table 4.

Data Availability Statement

The dataset compiled from Musso et al. (2022b) is accessible on PANGEA (Musso et al., 2022a). Data collected from both Maier and van Meerveld (2021b) and Maier et al. (2021) is available on GFZ Data Services (Maier & van Meerveld, 2021a). Information regarding the evolution of soil (hydraulic) properties can be found in the data set on GFZ Data Services (Hartmann, Weiler, & Blume, 2020b). Data on soil moisture, isotope profiles, and trinary images of the dye tracer experiments is accessible at the GFZ data service (Hartmann et al., 2024).

Acknowledgments
This research has been supported by the German Research Foundation (DFG) and the Swiss National Science Foundation (SNF) within the DFG-SNF project Hillscape (Hillslope Chronosequence and Process Evolution) (DFG; Grant BL 1184/4-1). We thank Britta Kattenstroth and Jonas Zimmermann for their technical guidance and assistance in conducting the field campaigns and their leading role and support in conducting the large-scale irrigation experiments. We also thank Moritz Lesche, Jonas Freymüller, Franziska Röpke, Nina Zahn, Wibke Richter, Louisa Kanis, Peter Grosse, and Carlo Seehaus for their persevering assistance in the field. We thank Kraftwerke Oberhasli AG (KWO) for permission to conduct the fieldwork at the Stein Glacier forefield and the Canton Uri, the community Unterschächen, and Korporation Uri for permission to conduct the fieldwork at the Griessfirn forefield. We are very grateful to Thomas Michel and his team of the Alpin Center Sustenpass and Peter Luchs as well as Christine, Franz, and Matthias Stadler at Chammlialp for their support and kind hospitality. Open Access funding enabled and organized by Projekt DEAL.

References

Allen, R. G., Pereira, L. S., Raes, D., & Smith, M. (1998). *Crop evapotranspiration – Guidelines for computing crop water requirements – Fao irrigation and drainage paper 56*. (Tech. Rep.). Agriculture Organization of the United Nations. Retrieved from http://www.fao.org/3/x0490e/x0490e00.htm:FAO-Foodand

Angermann, L., Jackisch, C., Allroggen, N., Sprenger, M., Zehe, E., Tronicke, J., et al. (2017). Form and function in hillslope hydrology: Characterization of subsurface flow based on response observations. *Hydrology and Earth System Sciences*, *21*(7), 3727–3748. https://doi.org/10.5194/hess-21-3727-2017

Archer, N., Bonell, M., Coles, N., MacDonald, A., Auton, C., & Stevenson, R. (2013). Soil characteristics and landcover relationships on soil hydraulic conductivity at a hillslope scale: A view towards local flood management. *Journal of Hydrology*, *497*, 208–222. https://doi.org/10.1016/j.jhydrol.2013.05.043

Beckwith, C. W., Baird, A. J., & Heathwaite, A. L. (2003). Anisotropy and depth-related heterogeneity of hydraulic conductivity in a bog peat. I: Laboratory measurements. *Hydrological Processes*, *17*(1), 89–101. https://doi.org/10.1002/hyp.1116

Blöschl, G. (2016). Predictions in ungauged basins – Where do we stand? *Proceedings of the International Association of Hydrological Sciences*, *373*, 57–60. https://doi.org/10.5194/piahs-373-57-2016

Blume, T., Zehe, E., & Bronstert, A. (2009). Use of soil moisture dynamics and patterns at different spatio-temporal scales for the investigation of subsurface flow processes. *Hydrology and Earth System Sciences*, *13*(7), 1215–1233. https://doi.org/10.5194/hess-13-1215-2009

Bonetti, S., Wei, Z., & Or, D. (2021). A framework for quantifying hydrologic effects of soil structure across scales. *Communications Earth & Environment*, *2*(107), 1–10. https://doi.org/10.1038/s43247-021-00180-0

Boxleitner, M., Musso, A., Waroszewski, J., Malkiewicz, M., Maisch, M., Dahms, D., et al. (2017). Late Pleistocene – Holocene surface processes and landscape evolution in the central Swiss Alps. *Geomorphology*, *295*, 306–322. https://doi.org/10.1016/j.geomorph.2017.07.006

Branger, F., & McMillan, H. K. (2020). Deriving hydrological signatures from soil moisture data. *Hydrological Processes*, *34*(6), 1410–1427. https://doi.org/10.1002/hyp.13645

Brocca, L., Morbidelli, R., Melone, F., & Moramarco, T. (2007). Soil moisture spatial variability in experimental areas of central Italy. *Journal of Hydrology*, *333*(2), 356–373. https://doi.org/10.1016/j.jhydrol.2006.09.004

Bronstert, A., Niehoff, D., & Bürger, G. (2002). Effects of climate and land-use change on storm runoff generation: Present knowledge and modelling capabilities. *Hydrological Processes*, *16*(2), 509–529. https://doi.org/10.1002/hyp.326

Chason, D. B., & Siegel, D. I. (1986). Hydraulic conductivity and related properties of peat, lost river peatland, northern Minnesota. *Soil Science*, *142*(2), 91–99. https://doi.org/10.1097/00010694-198608000-00005

Clothier, B. E., Green, S. R., & Deurer, M. (2008). Preferential flow and transport in soil: Progress and prognosis. *European Journal of Soil Science*, *59*(1), 2–13. https://doi.org/10.1111/j.1365-2389.2007.00991.x

Conen, F., Yakutin, M. V., Zumbrunn, T., & Leifeld, J. (2007). Organic carbon and microbial biomass in two soil development chronosequences following glacial retreat. *European Journal of Soil Science*, *58*(3), 758–762. https://doi.org/10.1111/j.1365-2389.2006.00864.x

Costantini, E. A. & Dazzi, C. (Eds.). (2013). *The soils of Italy* (1st ed., p. 354). Springer Science+Business Media. https://doi.org/10.1007/978-94-007-5642-7

Crocker, R. L., & Major, J. (1955). Soil development in relation to vegetation and surface age at Glacier Bay, Alaska. *Journal of Ecology*, *43*(2), 427–448. https://doi.org/10.2307/2257005

Cui, L., Li, G., Chen, Y., & Li, L. (2021). Response of landscape evolution to human disturbances in the coastal wetlands in northern Jiangsu province, China. *Remote Sensing*, *13*(11), 2030. https://doi.org/10.3390/rs13112030

D'Amico, M. E., Freppaz, M., Filippa, G., & Zanini, E. (2014). Vegetation influence on soil formation rate in a proglacial chronosequence (Lys Glacier, NW Italian Alps). *CATENA*, *113*, 122–137. https://doi.org/10.1016/j.catena.2013.10.001

Demir, Y., & Doğan Demir, A. (2019). The effect of organic matter applications on the saturated hydraulic conductivity and available water-holding capacity of sandy soils. *Applied Ecology and Environmental Research*, *17*(2), 3137–3146. https://doi.org/10.15666/aeer/1702_31373146

Douglass, D. C., & Bockheim, J. G. (2006). Soil-forming rates and processes on quaternary moraines near Lago Buenos Aires, Argentina. *Quaternary Research*, *65*(02), 293–307. https://doi.org/10.1016/j.yqres.2005.08.027

Dümig, A., Smittenberg, R., & Kögel-Knabner, I. (2011). Concurrent evolution of organic and mineral components during initial soil development after retreat of the Damma Glacier, Switzerland. *Geoderma*, *163*(1), 83–94. https://doi.org/10.1016/j.geoderma.2011.04.006

Egli, M., Filip, D., Mavris, C., Fischer, B., Götze, J., Raimondi, S., & Seibert, J. (2012). Rapid transformation of inorganic to organic and plant-available phosphorous in soils of a glacier forefield. *Geoderma*, *189–190*, 215–226. https://doi.org/10.1016/j.geoderma.2012.06.033

Egli, M., Fitze, P., & Mirabella, A. (2001). Weathering and evolution of soils formed on granitic, glacial deposits: Results from chronosequences of Swiss alpine environments. *CATENA*, *45*(1), 19–47. https://doi.org/10.1016/S0341-8162(01)00138-2

Egli, M., Mavris, C., Mirabella, A., & Giaccai, D. (2010). Soil organic matter formation along a chronosequence in the Morteratsch proglacial area (Upper Engadine, Switzerland). *CATENA*, *82*(2), 61–69. https://doi.org/10.1016/j.catena.2010.05.001

Egli, M., Mirabella, A., & Sartori, G. (2008). The role of climate and vegetation in weathering and clay mineral formation in late quaternary soils of the Swiss and Italian alps. *Geomorphology*, *102*(3), 307–324. https://doi.org/10.1016/j.geomorph.2008.04.001

Egli, M., Wernli, M., Kneisel, C., & Haeberli, W. (2006). Melting glaciers and soil development in the proglacial area Morteratsch (Swiss alps): I. Soil type chronosequence. *Arctic Antarctic and Alpine Research - ARCT ANTARCT ALP RES*, *38*(4), 499–509. https://doi.org/10.1657/1523-0430(2006)38[499:MGASDI]2.0.CO;2

Ehret, U., Gupta, H. V., Sivapalan, M., Weijs, S. V., Schymanski, S. J., Blöschl, G., et al. (2014). Advancing catchment hydrology to deal with predictions under change. *Hydrology and Earth System Sciences*, *18*(2), 649–671. https://doi.org/10.5194/hess-18-649-2014

Ellenberg, H. H. (1988). *Vegetation ecology of central Europe* (p. 756). Cambridge University Press.

Fan, B., Liu, X., Zhu, Q., Qin, G., Li, J., Lin, H., & Guo, L. (2020). Exploring the interplay between infiltration dynamics and critical zone structures with multiscale geophysical imaging: A review. *Geoderma*, *374*, 114431. https://doi.org/10.1016/j.geoderma.2020.114431

Frey, F. (1965). Geologie der östlichen claridenkette. (Doctoral dissertation, ETH Zurich, Zürich). (SA aus: Vierteljahrsschrift der Naturforschenden Gesellschaft in Zürich, Jg.110, Heft 1, S.1-287. Diss. Naturwiss. ETH Zürich, Nr. 3590, 0000. RefTrümpy, R. ; Korref.: Gansser, A.). https://doi.org/10.3929/ethz-a-000088454

Ghestem, M., Sidle, R. C., & Stokes, A. (2011). The influence of plant root systems on subsurface flow: Implications for slope stability. *BioScience*, *61*(11), 869–879. https://doi.org/10.1525/bio.2011.61.11.6

Gnann, S. J., McMillan, H. K., Woods, R. A., & Howden, N. J. K. (2021). Including regional knowledge improves baseflow signature predictions in large sample hydrology. *Water Resources Research*, *57*(2), e2020WR028354. https://doi.org/10.1029/2020WR028354

Godsey, S., & Elsenbeer, H. (2002). The soil hydrologic response to forest regrowth: A case study from southwestern Amazonia. *Hydrological Processes*, *16*(7), 1519–1522. https://doi.org/10.1002/hyp.605

Goeking, S. A., & Tarboton, D. G. (2020). Forests and water yield: A synthesis of disturbance effects on streamflow and snowpack in western coniferous forests. *Journal of Forestry*, *118*(2), 172–192. https://doi.org/10.1093/jofore/fvz069

© Google Maps. (2020a). Griess firn map, 8751 spiringen, ch. Google Maps, January 2020, maps.google.com. (Kartendaten 2020, Maps).

© Google Maps. (2020b). Stone glacier map, 3863 gadmen, ch. Google Maps, April 2020, maps.google.com. (Pictures 2020 Flotron/Perinjaquet, Maxar Technologies, Maps).

Gralher, B., Herbstritt, B., Weiler, M., Wassenaar, L. I., & Stumpp, C. (2016). Correcting laser-based water stable isotope readings biased by carrier gas changes. *Environmental Science and Technology*, *50*(13), 7074–7081. https://doi.org/10.1021/acs.est.6b01124

Greinwald, K., Dieckmann, L. A., Schipplick, C., Hartmann, A., Scherer-Lorenzen, M., & Gebauer, T. (2021). Vertical root distribution and biomass allocation along proglacial chronosequences in central Switzerland. *Arctic Antarctic and Alpine Research*, *53*(1), 20–34. https://doi.org/10.1080/15230430.2020.1859720

Greinwald, K., Gebauer, T., Musso, A., & Scherer-Lorenzen, M. (2021). Similar successional development of functional community structure in glacier forelands despite contrasting bedrocks. *Journal of Vegetation Science*, *32*(2), e12993. https://doi.org/10.1111/jvs.12993

Greinwald, K., Gebauer, T., Treuter, L., Kolodziej, V., Musso, A., Maier, F., et al. (2021). Root density drives aggregate stability of soils of different moraine ages in the Swiss alps. *Plant and Soil*, *468*(1–2), 439–457. https://doi.org/10.1007/s11104-021-05111-8

Haeberli, W. (2017). Integrative modelling and managing new landscapes and environments in de-glaciating mountain ranges: An emerging trans-disciplinary research field. *Forestry Research and Engineering: International Journal*, *1*(1), 00005. https://doi.org/10.15406/freij.2017.01.00005

Hahm, W. J., Riebe, C. S., Lukens, C. E., & Araki, S. (2014). Bedrock composition regulates mountain ecosystems and landscape evolution. *Proceedings of the National Academy of Sciences*, *111*(9), 3338–3343. https://doi.org/10.1073/pnas.1315667111

Hartmann, A., Semenova, E., Weiler, M., & Blume, T. (2020). Field observations of soil hydrological flow path evolution over 10 millennia. *Hydrology and Earth System Sciences*, *24*(6), 3271–3288. https://doi.org/10.5194/hess-24-3271-2020

Hartmann, A., Weiler, M., & Blume, T. (2020a). The impact of landscape evolution on soil physics: Evolution of soil physical and hydraulic properties along two chronosequences of proglacial moraines. *Earth System Science Data*, *12*(4), 3189–3204. https://doi.org/10.5194/essd-12-3189-2020

Hartmann, A., Weiler, M., & Blume, T. (2020b). Soil physical and hydraulic properties along two chronosequences of proglacial moraines [dataset]. GFZ Data Services. https://doi.org/10.5880/GFZ.4.4.2020.004

Hartmann, A., Weiler, M., & Blume, T. (2024). Soil moisture response, stable water isotope profiles, and trinary images of vertical subsurface flow paths across the evolution of siliceous and calcareous soil in proglacial areas [dasaset]. *GFZ Data Services*. https://doi.org/10.5880/GFZ.4.4.2024.001

Hartmann, A., Weiler, M., Greinwald, K., & Blume, T. (2022). Subsurface flow paths in a chronosequence of calcareous soils: Impact of soil age and rainfall intensities on preferential flow occurrence. *Hydrology and Earth System Sciences*, *26*(19), 4953–4974. https://doi.org/10.5194/hess-26-4953-2022

He, L., & Tang, Y. (2008). Soil development along primary succession sequences on moraines of Hailuogou Glacier, Gongga Mountain, Sichuan, China. *CATENA*, *72*(2), 259–269. https://doi.org/10.1016/j.catena.2007.05.010

Heidbüchel, I., Troch, P. A., & Lyon, S. W. (2013). Separating physical and meteorological controls of variable transit times in zero-order catchments. *Water Resources Research*, *49*(11), 7644–7657. https://doi.org/10.1002/2012WR013149

Heikkinen, O., & Fogelberg, P. (1980). Bodenentwicklung im hochgebirge: Ein beispiel am vorfeld des steingletschers in der schweiz. *Geographica Helvicta*, *3*, 107–112. https://doi.org/10.5194/gh-35-107-1980

Hervé, M. (2018). Rvaidememoire: Testing and plotting procedures for biostatistics. R package version 0.9-69, 3.

IAEA/WMO. (2021). *Global network of isotopes in precipitation* (Tech. Rep.). The GNIP Database. Retrieved from http://www.iaea.org/water

IUSS Working Group WRB. (2014). *World reference base for soil resources*. World Soil Resources Reports.

Ivy-Ochs, S., Kerschner, H., Reuther, A., Preusser, F., Heine, K., Maisch, M., et al. (2008). Chronology of the last glacial cycle in the European alps. *Journal of Quaternary Science*, *23*(6–7), 559–573. https://doi.org/10.1002/jqs.1202

Jarvis, N., Koestel, J., Messing, I., Moeys, J., & Lindahl, A. (2013). Influence of soil, land use and climatic factors on the hydraulic conductivity of soil. *Hydrology and Earth System Sciences*, *17*(12), 5185–5195. https://doi.org/10.5194/hess-17-5185-2013

Jefferson, A., Grant, G., Lewis, S., & Lancaster, S. (2010). Coevolution of hydrology and topography on a basalt landscape in the Oregon cascade range, USA. *Earth Surface Processes and Landforms*, *35*(7), 803–816. https://doi.org/10.1002/esp.1976

Jenny, H. (1941). *Factors of soil formation: A system of quantitative pedology* (Dover Publications ed.). McGraw-Hill.

Jin, Z., Zhao, Q., Qin, X., Zhang, J., Zhang, H., Qin, J., et al. (2021). Quantifying the impact of landscape changes on hydrological variables in the alpine and cold region using hydrological model and remote sensing data. *Hydrological Processes*, *35*(10), e14392. https://doi.org/10.1002/hyp.14392

Khaleel, R., Reddy, K. R., & Overcash, M. R. (1981). Changes in soil physical properties due to organic waste applications: A review. *Journal of Environmental Quality*, *10*(2), 133–141. https://doi.org/10.2134/jeq1981.00472425001000020002x

Kim, S. (2009). Characterization of soil moisture responses on a hillslope to sequential rainfall events during late autumn and spring. *Water Resources Research*, *45*(9), W09425. https://doi.org/10.1029/2008WR007239

Kirkby, M. (1988). Hillslope runoff processes and models. *Journal of Hydrology*, *100*(1), 315–339. https://doi.org/10.1016/0022-1694(88)90190-4

Leimer, S., Berner, D., Birkhofer, K., Boeddinghaus, R. S., Fischer, M., Kandeler, E., et al. (2021). Land-use intensity and biodiversity effects on infiltration capacity and hydraulic conductivity of grassland soils in southern Germany. *Ecohydrology*, *14*(6), e2301. https://doi.org/10.1002/eco.2301

Lin, H. (2003). Hydropedology: Bridging disciplines, scales, and data. *Vadose Zone Journal*, *2*, 1–11. https://doi.org/10.2113/2.1.1

Litwin, D. G., Tucker, G. E., Barnhart, K. R., & Harman, C. J. (2022). Groundwater affects the geomorphic and hydrologic properties of coevolved landscapes. *Journal of Geophysical Research: Earth Surface*, *127*(1), e2021JF006239. https://doi.org/10.1029/2021JF006239

Lohse, K. A., & Dietrich, W. E. (2005). Contrasting effects of soil development on hydrological properties and flow paths. *Water Resources Research*, *41*(12), W12419. https://doi.org/10.1029/2004WR003403

Maeda, K., Tanaka, T., Park, H., & Hattori, S. (2006). Spatial distribution of soil structure in a suburban forest catchment and its effect on spatio-temporal soil moisture and runoff fluctuations. *Journal of Hydrology*, *321*(1), 232–256. https://doi.org/10.1016/j.jhydrol.2005.08.003

Maier, F., & van Meerveld, I. (2021a). Hillscape project - Data on moraine soil properties and on overland flow and subsurface flow characteristics [Dataset]. GFZ Data Services. https://doi.org/10.5880/fidgeo.2021.011

Maier, F., & van Meerveld, I. (2021b). Long-term changes in runoff generation mechanisms for two proglacial areas in the Swiss alps I: Overland flow. *Water Resources Research*, *57*(12), e2021WR030221. https://doi.org/10.1029/2021WR030221

Maier, F., van Meerveld, I., Greinwald, K., Gebauer, T., Lustenberger, F., Hartmann, A., & Musso, A. (2020). Effects of soil and vegetation development on surface hydrological properties of moraines in the Swiss alps. *CATENA*, *187*, 104353. https://doi.org/10.1016/j.catena.2019.104353

Maier, F., van Meerveld, I., & Weiler, M. (2021). Long-term changes in runoff generation mechanisms for two proglacial areas in the Swiss alps II: Subsurface flow. *Water Resources Research*, *57*(12), e2021 WR030223. https://doi.org/10.1029/2021WR030223

Mangiafico, S. S. (2016). *Summary and analysis of extension program evaluation in R* (Vol. 125, pp. 16–22). Rutgers Cooperative Extension.

McGee, D., de Menocal, P., Winckler, G., Stuut, J., & Bradtmiller, L. (2013). The magnitude, timing and abruptness of changes in north African dust deposition over the last 20,000 yr. *Earth and Planetary Science Letters*, *371–372*, 163–176. https://doi.org/10.1016/j.epsl.2013.03.054

MeteoSwiss. (2020a). *Climate normals Grimsel Hospiz reference period 1981–2010*. Federal Office of Meteorology and Climatology MeteoSwiss. Retrieved from https://www.meteoswiss.admin.ch/product/output/climate-data/climate-diagrams-normal-values-station-processing/GRH/climsheet_GRH_np8110_e.pdf

MeteoSwiss. (2020b). *Climate normals Pilatus 1981–2010, referene period 1981–2010*. Federal Office of Meteorology and Climatology MeteoSwiss. Retrieved from https://www.meteoswiss.admin.ch/product/output/climate-data/climate-diagrams-normal-values-station-processing/PIL/climsheet_PIL_np8110_e.pdf

Montagne, D., & Cornu, S. (2010). Do we need to include soil evolution module in models for prediction of future climate change? *Climatic Change*, *98*(1), 75–86. https://doi.org/10.1007/s10584-009-9666-3

Müller, M. H., Alaoui, A., Kuells, C., Leistert, H., Meusburger, K., Stumpp, C., et al. (2014). Tracking water pathways in steep hillslopes by δ^{18}o depth profiles of soil water. *Journal of Hydrology*, *519*(Part A), 340–352. https://doi.org/10.1016/j.jhydrol.2014.07.031

Musso, A., Ketterer, M. E., Greinwald, K., Geitner, C., & Egli, M. (2020). Rapid decrease of soil erosion rates with soil formation and vegetation development in periglacial areas. *Earth Surface Processes and Landforms*, *45*(12), 2824–2839. https://doi.org/10.1002/esp.4932

Musso, A., Lamorski, K., Sławiński, C., Geitner, C., Hunt, A., Greinwald, K., & Egli, M. (2019). Evolution of soil pores and their characteristics in a siliceous and calcareous proglacial area. *CATENA*, *182*, 104154. https://doi.org/10.1016/j.catena.2019.104154

Musso, A., Tikhomirov, D., Plötze, M. L., Greinwald, K., Hartmann, A., Geitner, C., et al. (2022a). Soil chemical and mineralogical data from moraine chronosequences of the proglacial areas of Stein glacier (Sustenpass) and Griess glacier (Klausenpass) in the Swiss Alps [Dataset]. PANGAEA. https://doi.org/10.1594/PANGAEA.949699

Musso, A., Tikhomirov, D., Plötze, M. L., Greinwald, K., Hartmann, A., Geitner, C., et al. (2022b). Soil formation and mass redistribution during the holocene using meteoric ^{10}Be, soil chemistry and mineralogy. *Geosciences*, *12*(2), 99. https://doi.org/10.3390/geosciences12020099

Nahar, N., Govindaraju, R., Corradini, C., & Morbidelli, R. (2004). Role of run-on for describing field-scale infiltration and overland flow over spatially variable soils. *Journal of Hydrology*, *286*(1), 36–51. https://doi.org/10.1016/j.jhydrol.2003.09.011

Nippgen, F., McGlynn, B. L., Emanuel, R. E., & Vose, J. M. (2016). Watershed memory at the Coweeta Hydrologic Laboratory: The effect of past precipitation and storage on hydrologic response. *Water Resources Research*, *52*(3), 1673–1695. https://doi.org/10.1002/2015WR018196

Pachepsky, Y., & Van Genuchten, M. (2011). Pedotransfer functions. In J. Glinski, J. Horabik, & J. Lipiec (Eds.), *Encyclopedia of agrophysics* (pp. 556–561). Springer. https://doi.org/10.1007/978-90-481-3585-1_109

Pertassek, T., Peters, A., & Durner, W. (2015). *Hyprop-fit software user's manual*. v. 3.0. UMS GmbH.

Pfister, L., Martínez-Carreras, N., Hissler, C., Klaus, J., Carrer, G. E., Stewart, M. K., & McDonnell, J. J. (2017). Bedrock geology controls on catchment storage, mixing, and release: A comparative analysis of 16 nested catchments. *Hydrological Processes*, *31*(10), 1828–1845. https://doi.org/10.1002/hyp.11134

Pornon, A., & Doche, B. (1996). Age structure and dynamics of rhododendron ferrugineum l. populations in the northwestern French alps. *Journal of Vegetation Science*, *7*(2), 265–272. https://doi.org/10.2307/3236327

Ramírez, B. H., van der Ploeg, M., Teuling, A. J., Ganzeveld, L., & Leemans, R. (2017). Tropical Montane Cloud Forests in the Orinoco river basin: The role of soil organic layers in water storage and release. *Geoderma*, *298*, 14–26. https://doi.org/10.1016/j.geoderma.2017.03.007

Rawls, W., Pachepsky, Y., Ritchie, J., Sobecki, T., & Bloodworth, H. (2003). Effect of soil organic carbon on soil water retention. *Geoderma*, *116*(1), 61–76. https://doi.org/10.1016/S0016-7061(03)00094-6

R Core Team. (2017). R: A language and environment for statistical computing. [Computer software manual]. https://www.R-project.org/

Ross, M. R. V., Nippgen, F., McGlynn, B. L., Thomas, C. J., Brooks, A. C., Shriver, R. K., et al. (2021). Mountaintop mining legacies constrain ecological, hydrological and biogeochemical recovery trajectories. *Environmental Research Letters*, *16*(7), 075004. https://doi.org/10.1088/1748-9326/ac09ac

Sajikumar, N., & Remya, R. (2015). Impact of land cover and land use change on runoff characteristics. *Journal of Environmental Management*, *161*, 460–468. https://doi.org/10.1016/j.jenvman.2014.12.041

Sauer, D., Finke, P., Sørensen, R., Sperstad, R., Schülli-Maurer, I., Høeg, H., & Stahr, K. (2012). Testing a soil development model against southern Norway soil chronosequences. *Quaternary International*, *265*, 18–31. https://doi.org/10.1016/j.quaint.2011.12.018

Schaetzl, R. J. (2002). A spodosol-entisol transition in northern Michigan. *Soil Science Society of America Journal*, *66*(4), 1272–1284. https://doi.org/10.2136/sssaj2002.1272

Scherrer, P., & Pickering, C. M. (2005). Recovery of alpine vegetation from grazing and drought: Data from long-term photoquadrats in Kosciuszko national park, Australia. *Arctic Antarctic and Alpine Research*, *37*(4), 574–584. https://doi.org/10.1657/1523-0430(2005)037[0574:ROAVFG]2.0.CO;2

Schimmelpfennig, I., Schaefer, J. M., Akçar, N., Koffman, T., Ivy-Ochs, S., Schwartz, R., et al. (2014). A chronology of holocene and little ice age glacier culminations of the Steingletscher, central alps, Switzerland, based on high-sensitivity beryllium-10 moraine dating. *Earth and Planetary Science Letters*, *393*, 220–230. https://doi.org/10.1016/j.epsl.2014.02.046

Šimůnek, J., van Genuchten, M. T., & Šejna, M. (2016). Recent developments and applications of the hydrus computer software packages. *Vadose Zone Journal*, *15*(7), vzj2016.04.0033. https://doi.org/10.2136/vzj2016.04.0033

Singh, N. K., Emanuel, R. E., McGlynn, B. L., & Miniat, C. F. (2021). Soil moisture responses to rainfall: Implications for runoff generation. *Water Resources Research*, *57*(9), e2020WR028827. https://doi.org/10.1029/2020WR028827

Stumpp, C., Stichler, W., Kandolf, M., & Šimůnek, J. (2012). Effects of land cover and fertilization method on water flow and solute transport in five lysimeters: A long-term study using stable water isotopes. *Vadose Zone Journal*, *11*(1), vzj2011.0075. https://doi.org/10.2136/vzj2011.0075

Tian, J., Zhang, B., He, C., & Yang, L. (2017). Variability in soil hydraulic conductivity and soil hydrological response under different land covers in the mountainous area of the Heihe river watershed, northwest China. *Land Degradation & Development*, *28*(4), 1437–1449. https://doi.org/10.1002/ldr.2665

Treter, U., Ramsbeck-Ullmann, M., Böhmer, H. J., & Bösche, H. (2002). Vegetationsdynamik im vorfeld des lysgletschers (valle di gressoney/region aosta/italien) seit 1821. *Erdkunde*, *56*(3), 2563–3267.

Troch, P. A., Lahmers, T., Meira, A., Mukherjee, R., Pedersen, J. W., Roy, T., & Valdés-Pineda, R. (2015). Catchment coevolution: A useful framework for improving predictions of hydrological change? *Water Resources Research*, *51*(7), 4903–4922. https://doi.org/10.1002/2015WR017032

Truong, N. C. Q., Khoi, D. N., Nguyen, H. Q., & Kondoh, A. (2022). Impact of forest conversion to agriculture on hydrologic regime in the large basin in Vietnam. *Water*, *14*(6), 854. https://doi.org/10.3390/w14060854

van der Meij, W., Temme, A., Lin, H., Gerke, H., & Sommer, M. (2018). On the role of hydrologic processes in soil and landscape evolution modeling: Concepts, complications and partial solutions. *Earth-Science Reviews*, *185*, 1088–1106. https://doi.org/10.1016/j.earscirev.2018.09.001

Van Genuchten, M. (1980). A closed-form equation for predicting the hydraulic conductivity of unsaturated soils. *Soil Science Society of America Journal*, *44*(5), 892–898. https://doi.org/10.2136/sssaj1980.03615995004400050002x

Vilmundardóttir, O. K., Gísladóttir, G., & Lal, R. (2014). Early stage development of selected soil properties along the proglacial moraines of Skaftafellsjökull glacier, se-Iceland. *CATENA*, *121*, 142–150. https://doi.org/10.1016/j.catena.2014.04.020

Wassenaar, L., Hendry, M., Chostner, V., & Lis, G. (2008). High resolution pore water d2h and d18o measurements by H_2O(liquid)–H_2O(vapor) equilibration laser spectroscopy. *Environmental Science and Technology*, *42*(24), 9262–9267. https://doi.org/10.1021/es802065s

Weiler, M. (2001). *Mechanisms controlling macropore flow during infiltration dye tracer experiments and simulations*. (Doctoral dissertation). Swiss Federal Institute of Technology Zurich. https://doi.org/10.3929/ethz-a-004180115

Wilson, D. J., Western, A. W., & Grayson, R. B. (2004). Identifying and quantifying sources of variability in temporal and spatial soil moisture observations. *Water Resources Research*, *40*(2), W02507. https://doi.org/10.1029/2003WR002306

Wlostowski, A. N., Molotch, N., Anderson, S. P., Brantley, S. L., Chorover, J., Dralle, D., et al. (2021). Signatures of hydrologic function across the critical zone observatory network. *Water Resources Research*, *57*(3), e2019WR026635. https://doi.org/10.1029/2019WR026635

Wojcik, R., Eichel, J., Bradley, J. A., & Benning, L. G. (2021). How allogenic factors affect succession in glacier forefields. *Earth-Science Reviews*, *218*, 103642. https://doi.org/10.1016/j.earscirev.2021.103642

Wojkowski, J., Wałega, A., Radecki-Pawlik, A., Młyński, D., & Lepeška, T. (2022). The influence of land cover changes on landscape hydric potential and river flows: Upper vistula, western Carpathians. *CATENA*, *210*, 105878. https://doi.org/10.1016/j.catena.2021.105878

Yang, F., Zhang, G.-L., Yang, J.-L., Li, D.-C., Zhao, Y.-G., Liu, F., et al. (2014). Organic matter controls of soil water retention in an alpine grassland and its significance for hydrological processes. *Journal of Hydrology*, *519*, 3086–3093. https://doi.org/10.1016/j.jhydrol.2014.10.054

Yang, Y., Fang, J., Ji, C., & Han, W. (2009). Above- and belowground biomass allocation in Tibetan grasslands. *Journal of Vegetation Science*, *20*(1), 177–184. https://doi.org/10.1111/j.1654-1103.2009.05566.x

Yang, Y., Xiao, H., Wei, Y., Zhao, L., Zou, S., Yang, Q., & Yin, Z. (2012). Hydrological processes in the different landscape zones of alpine cold regions in the wet season, combining isotopic and hydrochemical tracers. *Hydrological Processes*, *26*(10), 1457–1466. https://doi.org/10.1002/hyp.8275

Yoshida, T., & Troch, P. A. (2016). Coevolution of volcanic catchments in Japan. *Hydrology and Earth System Sciences*, *20*(3), 1133–1150. https://doi.org/10.5194/hess-20-1133-2016

Zapata-Rios, X., Brooks, P. D., Troch, P. A., McIntosh, J., & Guo, Q. (2016). Influence of terrain aspect on water partitioning, vegetation structure and vegetation greening in high-elevation catchments in northern New Mexico. *Ecohydrology*, *9*(5), 782–795. https://doi.org/10.1002/eco.1674

Zimmermann, B., Elsenbeer, H., & De Moraes, J. M. (2006). The influence of land-use changes on soil hydraulic properties: Implications for runoff generation. *Forest Ecology and Management*, *222*(1), 29–38. https://doi.org/10.1016/j.foreco.2005.10.070